Transgene-free hematopoietic stem and progenitor cells from human induced pluripotent stem cells.

Laurence Guyonneau-Harmand[1,2,3], Bruno L'Homme[4], Brigitte Birebent[3], Christophe Desterke[5,6], Nathalie Chevallier[3,7,8], Loïc Garçon[1,2], Hélène Lapillonne[1,2,9], Marc Benderitter[4], François Delhommeau[1,2], Thierry Jaffredo[10]*, Alain Chapel[1,2,4]* and Luc Douay[1,2,3,9]

[1] UPMC Univ Paris 06, UMR_S938 CDR Saint-Antoine, Prolifération et Différenciation des Cellules Souches, F-75012 Paris, France.

[2] INSERM, UMR_S938, Prolifération et Différenciation des Cellules Souches, F-75012 Paris, France.

[3] EFS Ile de France, Unité d'Ingénierie et de Thérapie Cellulaire, Créteil, F-94017, France.

[4] IRSN, PRP-HOM, SRBE, Laboratoire de recherche en régénération des tissus sains irradiés (LR2I), F-92262 Fontenay-aux-Roses, France.

[5] University Paris Sud 11, UFR Medecine, Villejuif FRANCE

[6] INSERM Unit UMS-33, bioinformatics plateform, Villejuif FRANCE

[7] Institut Mondor de Recherche Biomédicale, INSERM U955-E10, Créteil, France,

[8] Université Paris Est, Faculté de Medecine, Créteil, France

[9] AP-HP, Hôpital St Antoine/Trousseau, Service d'Hématologie Biologique, F- 75012 Paris, France.

[10] Sorbonne Universités, UPMC Univ Paris 06, CNRS UMR7622, Inserm U 1156, IBPS, Laboratoire de Biologie du Développement; 75005 Paris

*Correspondence to: thierry.jaffredo@upmc.fr; alain.chapel@irsn.fr

Introductory paragraph:

The successful production of Hematopoietic Stem and Progenitor Cells (HSPCs) from human pluripotent sources is conditioned by transgene delivery[1-5]. We describe here a dedicated and tractable one step, GMP-grade, transgene-free and stroma-free protocol to produce HSPCs from human induced pluripotent stem cells (hiPSCs). This procedure, applied to several sources of hiPSCs with equal efficiency, is based on a directed differentiation with morphogens and cytokines to generate a cell population close to nascent HSPCs or their immediate forerunners i.e., hemogenic endothelial cells[6-9]. Following engraftment into immunocompromised recipients, this cell population was proved capable of a robust myeloid, lymphoid and definitive red blood cell production in sequential recipients for at least 40 weeks. Further identification of the repopulating cells show that they express the G protein–coupled receptor APELIN (APLNR) and the homing receptor CXCR4. This demonstrates that the generation of *bona fide* HSPCs from hiPSCs without transgenes is possible and passes through an early endo-hematopoietic intermediate. This work opens the way to the generation of clinical grade HSPCs for the treatment of hematological diseases and holds promise for the analysis of HSPC development in the human species.

While in standard hiPSC differentiation protocols, $CD34^+CD45^+$ hematopoietic cells appeared from bursting Embryoid Bodies (EBs) at day 10 until day 14[1,5,10,11], here D17 EBs remained compact and spherical without burst therefore assessing a dramatic delay in differentiation (Fig. 1a). These culture conditions, reproducibly applied to three individual hiPSC lines, derived using different reprogramming protocols demonstrated the robustness of the method.

To determine the point of hemogenic endothelial cell (EC)/early HSPC commitment, we analyzed EBs by qRT-PCR on D3, 7, 9, 13, 15, 16 and 17 for the expression of 49 endothelial- and hematopoietic-specific genes, with $CD34^+$ cord blood (CB) HSPCs as a reference (Supplementary Table 1). Hierarchical clustering (Fig. 1b, and Supplementary Fig. 1) revealed two main groups, one associated with $CD34^+$ CB HSPCs and another one with D3 to D17 EBs. The latter displayed two distinct clusters: the early EBs (D3 to D13) and the late EBs (D15 to D17). Further analysis of the qRT-PCR identified D13 as the point of EC commitment based on CD309 (VEGFR2/FLK1) mRNA expression and D16 as hemogenic endothelial commitment/EHT based on RUNX1 mRNA expression (Fig. 1c) in keeping with developmental studies[12]. Early HSPC commitment was overt from D17 testified by the expression of ITGA2 (Integrin alpha-2), CEBPA (CCAAT enhancer binding protein alpha), the transcription factors c-MYB and SCL, this latter exhibiting a bimodal curve in keeping with its role on hemangioblast and hematopoietic commitment respectively[13], the TPO receptor MPL (Fig 1c). Flow cytometry indicated a decrease in CD309 (EC marker) expression from D13 to D17 and an increase of ITGA2, CKIT and MPL (early HSPC markers) expressions (Fig. 1d) in keeping with the qRT-PCR analysis (Fig. 1c).

We next evaluated the endothelial and hematopoietic potential of D15 to D17 EBs using dedicated *ex vivo* functional tests (Fig. 2a and Supplementary Table 2). D15 EBs displayed a

strong endothelial-forming potential since they generate endothelial colony-forming cells (CFCs) (Fig. 2a1), pseudo-microtubules (Fig. 2a2) and endothelial-like cells (Fig. 2a3)[14], but lacked hematopoietic-forming capacity, being unable to generate clonogenic colonies and displaying a low frequency of long term culture-initiating cells (Supplementary Table 2). In contrast D17 EBs lacked endothelial potential but showed an increased hematopoietic capacity (Fig. 2a4, a5), confirming hematopoietic commitment within this period.

D16 cells were probed *in vivo* by subcutaneous transplantation in Matrigel (growth factor reduced) plug with or without human Mesenchymal Stem Cells (hMSCs) into immunocompromised Foxn1$^{-/-}$ (nude) mice (Fig. 2b)[15]. Two weeks after transplantation, both human vascular and hematopoietic differentiation was found. Human vascular structures (Fig. 2c, d, e), made of human von Willebrand factor^{+} (Fig. 2d) and CD31^{+} (Fig. 2e) cells were detected in the graft seeded with D16 cells associated with (/) hMSCs. qRT-PCR revealed the expression of hVEGFR2, hENG (ENDOGLIN), hPECAM and hVE-CADHERIN in the D16 cells/hMSCs grafts and, as expected, in the endothelial progenitor cells/hMSCs grafts (Supplementary Fig. 2). Moreover, D16 cells/hMSCs grafts also expressed the CD45 antigen and human beta, gamma and epsilon globin transcripts, while D16 cell grafts alone expressed only human epsilon globin transcript disclosing a block of maturation (Supplementary Fig. 2). D16 EBs thus displayed a balanced endothelial-hematopoietic pattern in keeping with our *ex vivo* results.

Based on the newly-formed hematopoietic capability disclosed at D17, we transplanted 4×10^5 D17 cells intravenously into 30 sublethally irradiated (3.5 gray) 8-week-old immunocompromised mice for 20 weeks followed by a challenging secondary transplantation in similarly-treated immunocompromised recipients for 20 additional weeks and compared it

systematically to $CD34^+$ CB HSPCs (Fig. 3a, Supplementary Fig. 3a). Hematopoietic reconstitution quantified by the surface expression of hCD45, hCD43 and hCD34 (Fig. 3b and Supplementary Fig. 3b-l)[16] was evident in 30/30 primary recipients and quantitatively comparable to that of $CD34^+$ CB HSPCs (Fig. 3c and Supplementary Fig. 3b, c-e, j) with 20.3+/-2.9 % of $hCD45^+$ cells in total mouse BM mononucleated cells, i.e., more than 200 times the threshold of 0.1% usually considered as positive for human hematopoietic engraftment in NSG mice[17], and 12.2+/-1.5 % of $hCD43^+$ and 7.29+/-1.0 % of $hCD34^+$. $hCD45^+$ BM cells harbor several hematopoietic lineages including B and T lymphoid ($hCD19^+$ and $hCD3^+$ respectively) and myeloid ($hCD14^+$) (Supplementary Fig. 4a-d) whereas $hCD45^-$ BM cells harbor $hCD235a^+$ erythroid progenitors/precursors (Supplementary Fig. 4a-b, e-f). Sorted $hCD45^+$ blood cells displayed the same multilineage pattern (Supplementary Fig. 5a) indicating a peripheralization of the grafted cells comparable to results obtained with $CD34^+$ CB HSPCs. Their human origin was confirmed (n=30/30) by qRT-PCR using human-specific primers (Supplementary Fig. 4g,). A human-specific clonogenic hematopoietic assay on BM cells from the first recipient revealed an overall frequency of 17.5+/-4.3 clones out of 10^4 total BM cells (Fig. 3f) distributed into CFU-GEMM, BFU-E and CFU-GM colonies (Fig. 3g1, 2, 3) Cytospin analysis revealed mature macrophages, histiomonocytes, myelocytes and erythroblasts (Fig. 3h1, 2, 3). 7.10^6 BM cells from the primary recipient were challenged in a secondary (n=30) (Fig 3d, e and Supplementary Fig. 3f-i, k) and eventually a tertiary (n=3) recipient (Supplementary Fig. 3l). Human $CD45^+$ cells represented 12.6+/-3.9 % of the mononucleated BM cells at 20 weeks (Fig. 3d), indicating a sustained reconstitution capacity. Multilineage engraftment was found in 30/30 secondary mice (Fig. 3e, Supplementary Fig. 6a-e) and was comparable to the pattern obtained on secondary $CD34^+$ CB HSPCs transplants (Supplementary Fig. 3f-i, k and Supplementary Fig. 6). The

human CFCs cloning efficiency was 5.5+/-3.1 % in 10^4 total mouse BM cells, pointing to a robust and prolonged self-renewal potential (Fig. 3f-h). The human origin of the engrafted cells was confirmed as above (Supplementary Fig. 3g).

To ensure the functionality of the grafted cells, we analyzed the ability of the human erythroid precursors from mouse BM to undergo hemoglobin switching *in vivo* and tested the phenotype and the functionality of T cells. Cells from both primary and secondary recipients generated human erythroid progenitors displaying high amounts of β (respectively 39.51+/-4.95% and 36.61+/-5.86%) and γ globin (respectively 57.49+/-3.95% and 61.39+/-4.86%) while ε globin was dramatically reduced to respectively 3.0+/-1.2% and 2.1+/-1.1% of total globin (Fig. 3i), a hallmark of definitive erythrocytes. Peripheral blood $hCD3^+$ T cells displayed high amounts of TCRαβ (Fig. 3j) and low amounts of TCRγδ similar to thymic $hCD3^+$ cells (Supplementary Fig. 5b) reminiscent of normal T lymphopoiesis. B and T lymphopoiesis was revealed in spleen $CD45^+$ cells by the expression of TCRß and hCD19 and were found similar to $CD34^+$ CB HSPCs grafts (Supplementary Fig 5b). Thymus $hCD3^+$ T cells, tested on their ability to expand *ex vivo,* measured by CSFE-labeling, under hCD3 and hCD28 stimulation (Fig. 3k) displayed a high expansion capacity after 5 days, thereby demonstrating T cells functionality.

To further identify the reconstituting population, we focused on APLNR related to ECs[18] and HCs from human embryonic stem cells[19] and to the homing receptor CXCR4[20,21]. Differentiating EBs displayed an enhanced APLNR and CXCR4 expression from D7 to D17 with the emergence of a double stained population accounting for 32.1% of the cells at D17 (Fig 4a). Grafting efficiency at 20 weeks was directly proportional to the number of $APLNR^+$ cells (Fig 4b). Moreover, only $APLNR^+$ cells reconstituted hematopoiesis after 20 weeks with 6.6+/-1.9 % $hCD45^+$ mononucleated cells, 3.4+/-2.5 % $hCD43^+$ and 1.1+/-0.4 % $hCD34^+$ in 6/6 grafted

mice (Fig. 4c, Supplementary Fig. 7a) and displayed multilineage reconstitution (Supplementary Fig. 7b-c), Importantly, D17 APLNR$^+$ cells did not harbor any CD45$^+$ cell indicating that reconstitution was not harbored by hCD45$^+$ progenitors (Supplementary Fig. 7d). In contrast, APLNR$^-$ cells failed to significantly engraft in 4/4 mice with 0.08+/-0.01 % hCD45$^+$ cells in mouse BM (Figure 4c, Supplementary Fig 7a). The APLNR$^+$ fraction also exhibited a homogeneous population of ENG$^+$/TIE$^+$/CKIT$^+$ (Fig. 4d) described to enhance definitive hematopoiesis in mice[22]. We compared the molecular profiles of APLNR$^+$ and APLNR$^-$ cells to that of D15 and D17 EBs, to hiPSCs and to control CD34$^+$ CB HSPCs through the expression of the set of 49 genes (Supplementary Table 3). Principal component analysis (PCA) of the 49 mRNAs as variables and the six cell populations as observations revealed that the first component likely corresponded to the factor "hematopoietic differentiation" (44.9% of the variance) (Fig. 4e). Aiming to reveal the traits involved in the grafting potential, we compared by PCA the APLNR$^+$, D17 and CB HSPC populations to the APLNR$^-$ and hiPSC populations. The third component that accounted for 19.23% of the variance segregated two groups differing by their grafting potential (Fig. 4f). A statistical SAM test which measures the strength of the relationship between gene expression and a response variable pointed out 8 genes (FDR<10%) significantly up-regulated in the group unable to graft, among them endothelial genes as TEK, PECAM, and KDR (Fig. 4g).

Collectively, we show that the generation of long-term multipotent HSPCs supporting hematopoietic reconstitution and self-renewal *in vivo,* passes through an early differentiated cell expressing APLNR more likely an endothelial cell undergoing EHT or a newly formed HSPC. Since this study has been performed under GMP-grade conditions, it may be envisioned that pluripotent stem cells may become a prioritized source of cells for HSPC transplantation.

Figure Legends

Fig. 1: Phenotypic characterization of hiPSC-derived endo-hematopoietic differentiation *ex vivo*.

(a) Experimental scheme. HiPSCs were differentiated into EBs over 17 days with the continuous presence of growth factors and cytokines. EBs were characterized at different time points using q-PCR and flow cytometry. Images depicted representative EBs at D13 and 17 respectively.

(b) Hierarchical clustering summarizing the expression of the set of 49 genes characteristics of the endothelium, hemogenic endothelium and hematopoietic cells with time in D3, D7, D9, D13, D15 and D17 EBs and in CB $CD34^+$ HSPCs.

(c) Q-PCR patterns of genes representative of the EHT balance from D13 to D17 EB differentiation. For each gene, the fold change is the mean +/- SEM of 6 experiments

(d) Flow cytometry analysis of human CD309, ITGA2, MPL and CKIT expression at D13 and D17 of EB culture.

Fig. 2: Functional endothelio-hematopoietic profiling between D15 and D17.

(a) *Ex vivo* tests probing the presence of endothelial (1-3) and hematopoietic (4-5) progenitors in EBs with time. Dissociated D15-17 EBs generate (1) CFC-ECs, (2) pseudo-microtubules, (3) EC-like cells capable of several passages, (4) CFC, and (5) LTC-ICs.

(b) Experimental scheme for *in vivo* tests to probe the endothelial capacity of D16 cells.

(c) D16 cells/hMSCs plug section. Masson's trichrome staining.

(d) D16 cells/hMSCs plug section. Human von Willebrand $factor^+$ cells (blue) immunostaining.

(e) D16 cells/hMSCs plug section. Human $CD31^+$ immunostaining (red). Cell nuclei are counterstained by DAPI.

Fig. 3: *In vivo* engraftment of D17 EBs in immunocompromised mice.

(a) Experimental design.

(b) Representative flow cytometry analysis of human vs mouse $CD45^+$ cell engraftment in a BM primary recipient.

(c-d) Engraftment of $hCD34^+$ $hCD43^+$ and $hCD45^+$ HSPCs in primary (c) or secondary (d) mouse BM 20 weeks post graft. Data are the mean +/- SEM.

(e) Human hematopoietic lineage distribution in representative secondary recipients. Cells were gated on $hCD45^+$ expression for hCD33, hCD19 and hCD3 whereas hCD235a was analyzed on whole BM cells. Data are the mean +/- SEM.

(f) Clonogenic hematopoietic tests on BM cells isolated from primary and secondary recipients. Frequency of CFU-GM, BFU-E and CFU-GEMM colonies.

(g) Representative colonies of CFU-GEMM (1), BFU-E (2) and CFU-GM (3) from primary and secondary BM cells.

(h) Cytospins. May Grünwald-Giemsa staining of cells isolated from clonogenic tests performed on primary and secondary recipients. Mature macrophages (1), histiomonocytes (2), myelocytes (2) and erythroblasts (3).

(i) Human globin expression from CB $CD34^+$ HSPCs erythroid culture, from BM primary and secondary recipients and BFU-E from BM primary recipients. Data are mean +/- SEM.

(j) Maturation of human T cells. Peripheral blood stained with antibodies against hTCR αβ and hTCR γδ, the cells are first gated on hCD3 and analyzed for TCR expression.

(k) Functionality of human T cells. The whole thymus population is CFSE labeled at D0 and gated on $hCD3^+$ expression (green). At D5, the unstimulated population is red while the stimulated parent population is blue.

Figure 4: Functional and molecular characterization of the $APLNR^+$ population.

(a) Flow cytometry analysis of APLNR and CXCR4 expression from D7 to D17 EB culture.

(b) Correlation between the percentage of $APLNR^+$ cells in the graft to those of $hCD45^+$ cells in the NOD-SCID BM primary recipients, 18weeks post-graft.

(c) Engraftment capacities of the $APNLR^+$ (n=6, red dots) and $APNLR^-$ (n=4, grey triangles) populations. Cells containing the reconstitution potential are within the $APLNR^+$ population. Data are expressed as the mean +/- SEM percentages of human engraftment, 18 weeks after transplant.

(d) Combinatorial flow cytometry analysis of the $APLNR^+$ population using CD45, TIE, ENG and CKIT anti-human antibodies.

(e) PCA with the set of 49 mRNAs as variables and the six cell populations as observations. PC1 versus PC2 score plot. The PC1 dimension likely corresponds to the trait « hematopoietic differentiation » which accounts for 44.9% of the variance. HiPSCs are segregated from the other populations on the second component which accounts for 24% of the variance.

(f) PCA with the set of 49 mRNAs as variables and the populations endowed or not with grafting potential. The PC3 dimension which accounts for 19.23% of the variance segregates the two groups.

(g) Heat map of the genes permitting the segregation of the two groups in (f).

Materials and Methods:

hiPSC amplification

The study was conducted using three different hiPSC lines: the FD136-25 (skin primary fibroblasts), reprogrammed with retroviral vectors and Thomson's combination (endogenous expression of Oct4, Sox2, Nanog and Lin28); the Pci-1426 and Pci-1432 lines (peripheral blood mononuclear cells-Phenocell) reprogrammed with episomes (Sox2, Oct4, KLF, cMyc). hiPSCs were maintained on CellStart (Invitrogen, Carlsbad, USA) in TESR2 medium (Stem Cell Technologies, Bergisch Gladbach, Germany) and the cells were passaged 1:6 onto freshly coated plates every 5 days using standard clump passaging with TRYple select (Invitrogen).

EB differentiation

EB differentiation was induced as previously described. After 24h, cells were transferred into differentiation medium (Lapillonne et al., 2010) containing 22 ng/mL of SCF, 20 ng/mL of TPO, 300 ng/mL of FLT3, 22 ng/mL of BMP4, 200 ng/mL of VEGF, 50 ng/mL of IL3, 50 ng/mL of IL6, 5 ng/mL of IL1, 100 ng/mL of GCSF, 50 ng/mL of IGF1 (PeproTech, Neuilly-sur-Seine, France). Medium was changed every other day.

Colony assays

At the indicated times, $1x10^5$ dissociated EBs or $3x10^4$ cells from xenotransplanted recipient BM were plated into 3 mL of complete methylcellulose medium in the presence of SCF, IL-3, EPO and GM-CSF (PeproTech, Neuilly-sur-Seine, France). As G-CSF also stimulates mouse progenitors, it was replaced by granulocyte-macrophage colony-stimulating factor (GM-CSF).

Aliquots (1 mL) of the mix were distributed into one 30 mm dish twice and maintained in a humidified chamber for 14 days. Colony-forming Cells (CFC) were scored on day 14.

Long-term culture-initiating cell assays

Long-term culture-initiating cell (LTC-IC) assays were performed as described previously (*35*), 15–100,000 cells/well on day 17 for the EBs and on day 0 for the control CD34+. Absolute LTC-IC counts corresponded to the cell concentrations, yielding 37% negative wells using Poisson statistics.

Pseudo-microtubules and EPC-like cells

For Pseudo-microtubules formation, cells were transferred onto growth factor reduced Matrigel (Corning) and culture in EGM2 medium (Lonza).

For EPC-like cells generation, cells were first plated on gelatin and cultured in EBM2 (Lonza) and split several times, after the first passaged the gelatin was no longer mandatory.

Flow cytometry

Staining of BM cells or dissociated EBs was performed with $2x10^5$ cells in 100 µL staining buffer (PBS containing 2% FBS) with 5:100 dilution of each antibody, for 20 min at room temperature in the dark. Data acquisition was performed on a Becton Dickinson Canto II cytometer.

In vivo analyses of angiogenesis potential

Foxn1−/− nude mice (Charles River, L'Abresle, France) were housed in the IMRB animal care facility. All experiments and procedures were performed in compliance with the French Ministry of Agriculture regulations for animal experimentation and approved by the local ethics committee.

In vivo assessment of the endothelial and hematopoietic potentials were probed on 9 nude mice. 1.750 10^6 D16 single cells or hEPCs and 1.750 10^6 hMSCs were mixed with 100µl of Matrigel phenol red free and growth factor reduced (Corning) and subcutaneously injected into the back of nude mice (two different plugs/ mouse). The controls were performed similarly but with 3.5 10^6 hMSCs or D16 single cells or hEPCs; for each condition n=3. Two weeks later, mice were sacrificed, the matrigel plug dissected out and cut into two parts. One part was processed for paraffin sectioning. Sections were deparaffinized, hydrated and stained whether with Masson's trichrome, a three-color protocol comprising nuclear staining with hematoxylin, cytoplasmic staining with acid fuchsin/xykidine ponceau and collagen staining with Light Green SF (all from VWR); or whether with an anti human Von Willebrand factor antibody (Dako), staining was developed with histogreen substrate (Abcys) and counterstained with Fast nuclear red (DakoCytomation), dehydrated and mounted, or wether with hCD31 (R&D system) as primary antibody and donkey anti-rabbit Cy3 (Jackson ImmunoResearch) as secondary antibody and DAPI and mounted with fluoromount G.

Sorting of APLNR positive cells

Cells were stained with the antibody hAPJ-APC clone 72133 (R&D systems) as described above. Sorting was carried out on a Moflo ASTRIOS Beckman Coulter apparatus and the purity was 98.1% APLNR^{+} cells.

Mouse transplantation

NOD/SCID-LtSz-scid/scid (NOD/SCID) and NOD.Cg-Prkdc^{scid}Il2rg^{tm1Wjl}/SzJ (NSG) (Charles River, L'Abresle, France) were housed in the IRSN animal care facility. All experiments and procedures were performed in compliance with the French Ministry of Agriculture regulations for animal experimentation and approved by the local ethics committee.

Mice, 6-8 weeks old and raised under sterile conditions, were sublethally irradiated with 3.5 Grays from a 137Cs source (2.115 Gy/min) 24 h before cell injection. To ensure consistency between experiments, only male mice were used. Prior to transplantation, the mice were temporarily sedated with an intraperitoneal injection of ketamine and xylazine. Cells (4 x10^{5} per mouse) were transplanted by retro-orbital injection in a volume of 100 µL using a 28.5 gauge insulin needle. A total of 147 mice were used in this study.

For the engraftment potential of the D17 cells on the three different hiPSC lines:

86 NSG mice were used as followed: 30 primary recipients, 30 secondary recipients and 26 as control.

48 NOD-SCID mice were used as followed: 20 primary recipients and 16 secondary recipients, 3 tertiary recipients and 9 as control.

For the engraftment potential of APLNR^{+} and APLNR^{-} population: 10 NOD-SCID mice were used and 3 NOD-SCID as control.

Assessment of human cell engraftment

Mice were sacrificed at week 12, 18 or 20. Femurs, tibias, liver, spleen and thymus were removed. Single cell suspensions were prepared by standard flushing and aliquots containing $1x10^6$ cells were stained in a total volume of 200µL staining buffer.

Samples were stained for engraftment assessment with the following markers: hCD45 clone J33, hCD43 clone DFT1, hCD34 clone 581 (Beckman Coulter) and hCD45 clone 5B1, mCD45 clone 30F11 (Miltenyi)

The BM of three mice were pooled to allow hCD45 microbead enrichment (Miltenyi), the multilineage was assessed using the following human markers : hCD3 clone UCHT1, hCD4 clone 13B8.2, hCD8 clone B9.11, hCD14 clone RMO52, hCD15 clone 80H5, hCD19 clone J3-119, hCD20 clone B9E9, hCD43 clone DFT1, hCD34-APC, hCD71 clone YDJ1.2.2 (all from Beckman Coulter antibodies, Brea, USA), CD45 clone 5B1 (Miltenyi), CD235a clone GA-R2 (Becton-Dickinson).

The blood samples of three mice were pooled to allow hCD45 microbead sorting (Miltenyi). The multilineage potential was assessed using the following human markers : hCD3 clone UCHT1, hCD4 clone 13B8.2, hCD8 clone B9.11, hCD14 clone RMO52, hCD15 clone 80H5, hCD11B Bear1, hCD19 clone J3-119, hCD20 clone B9E9, hIGM clone SA-DA4 (all from Beckman Coulter antibodies, Brea, USA).

Non-injected mouse BM was used as a control for non-specific staining.

Compensation was performed by the FMO method with anti-mouse Ig and data were acquired on a BD Canto II cytometer.

T-cell maturity and functionality assay

The presence of TCR αβ and TCR γδ in peripheral blood was assessed by flow cytometry using the following human markers : hCD3 clone UCHT1 (positive gating), TCR αβ clone IP26A and TCR γδ clone IMMU510 (all from Beckman Coulter antibodies, Brea, USA).

Thymus and spleen cells were isolated, CFSE labelled and seeded in cell culture media complemented or not with hCD3 and hCD28 (Beckman Coulter both 1µg/ml). After 5 days, cells were harvested and stained with anti-hCD3 clone UCHT1 and analyzed on a BD Canto II cytometer. FlowJo analysis software was used to gate on $CD3^+$ T-cells and generate the overlaid histogram plots.

Assessment of the APLNR cell safety

Three sub-lethally irradiated NOD/SCID mice were subcutaneously injected each with 3 million APLNR positive cells. No teratoma was found after 2 months follow-up according to FDA guidelines.

In addition, no tumor was macroscopically detected in any mouse after analysis of the organs (140/140 mice) or after microscopic analysis of different tissues (brain, lungs, kidneys, BM, liver and gut) (140/140 mice).

Quantitative PCR

Total mRNA was isolated with the RNA minikit (Qiagen, Courtaboeuf, France). mRNA integrity was checked on a Bioanalyzer 2100 (Agilent Technologies, Massy, France). cDNAs were constructed by reverse transcription with Superscript (Life Technologies, Carlsbad, USA). PCR assays were performed using a TaqMan PCR master mix (Life Technologies) and specific primers (Applied BioSystems, Carlsbad, USA) for selected genes (see table below), together

with a sequence detection system (QuantStudio™ 12K Flex Real-Time PCR System, Life Technologies). In each sample the fluorescent PCR signal of each target gene was normalized to the fluorescent signal of the housekeeping gene glyceraldehyde 3-phosphate dehydrogenase (GAPDH).

The human origin of the mRNAs from mouse BM was assessed by measuring hCD45, hCD15, hMPO, hITGA2 and hGAPDH. From CFCs post grafting and globin type expression in the mouse BM, we measured beta, gamma and epsilon globins using Taqman probes.

Controls were cultured erythroblasts generated from cord blood $CD34^{+}$.

Pluripotency genes	Hs01053049_s1	SOX2	**Endothelial genes**		Hs00945146_m1	TEK
	Hs00153408_m1	MYC			Hs00231079_m1	RUNX1
	Hs00702808_s1	LIN28A			Hs00911700_m1	KDR
	Hs04260366_g1	NANOG			Hs01574659_m1	NOS3
	Hs00358836_m1	KLF4				
	Hs00742896_s1	POU5F1	**Human housekeeping genes**		Hs00357333_g1 , Hs02758991_g1	Human beta actin Human GAPDH
Mouse housekeeping genes	Mm99999915_g1	Murine GAPDH				
Hematopoietic genes	Hs00924296_m1	MPO	Hs01076122_m1	DNTT	Hs00269972_s1	CEBPA
	Hs01106466_s1	FUT4	Hs00172743_m1	RORC	Hs01115556_m1	MITF
	Hs00174029_m1	cKIT	Hs00962186_m1	CD3G	Hs01029175_m1	NFIB
	Hs01116228_m1	ITGA2B	Hs00169777_m1	PECAM	Hs04188695_m1	HOPX
	Hs00766613_m1	APLNR	Hs00231119_m1	GATA2	Hs00171406_m1	HLF
	Hs00161700_m1	STIL	Hs00959427_m1	EPOR	Hs01070488_m1	RBPMS
	Hs00231119_m1	GATA2	Hs00610592_m1	KLF1	Hs00171569_m1	HMGA2
	Hs00995536_m1	BMI1	Hs01085823_m1	GATA1	Hs00223161_m1	PRDM16
	Hs00941830_m1	NCAM1	Hs04186042_m1	RUNX1	Hs01017441_m1	MEIS1
	Hs04189704_m1	PTPRC	Hs00176738_m1	MATK	Hs00414553_g1	NKX2-3
	Hs00174333_m1	CD19	Hs00180489_m1	MPL	Hs00971097_m1	MLLT3
	Hs00162150_m1	SPIB	Hs04334142_m1	FLI1	Hs00925052_m1	GATA3
	Hs00958474_m1	IKZF1	Hs00268388_s1	SOX4	Hs01128710_m1	IRF8
	Hs01851142_s1	RAG2	Hs00193527_m1	C-MYB	Hs00256884_m1	HOXB4
	Hs00266821_m1	HOXA9	Hs01554629_m1	ERG	Hs00610592_m1	KLF1
	Hs00931969_m1	RORA	Hs01547250_m1	LEF1	Hs04334142_m1	FLI1
	Hs00959427_m1	EPOR	Hs00176738_m1	MATK	Hs00180489_m1	MPL

Statistical analysis

All statistics were determined with R Software 3.1.1 (2014-07-10) (R Core Team, 2013), INGENUITY and SAM Software. Data are represented with hierarchical clustering and PCA.

References

H. Lapillonne *et al.*, Red blood cell generation from human induced pluripotent stem cells: perspectives for transfusion medicine. Haematologica. 95:1651-1659 (2010).

Aknowledgments:

We would like to thank Franck Chiappini for help in statistical analysis, Charles Durand for expert assistance with heat map and PCA analysis, Stéphane Viville for providing iPS line, Georges Tarlet, Christine Linard, Marianne Gervais-Taurel and Dhouha Darghouth for their technical support, Rima Haddad for her scientific support and Sophie Gournet for excellent drawing assistance. This work was supported by "Direction Générale de l'Armement" via the ASTRID/ANR program, the Etablissement Français du Sang (EFS) via the APR 2013 and the association "Combattre La Leucémie". These studies were supported by a joint grant from Agence Nationale pour la Recherche/California Institute for Regenerative Medicine (ANR/CIRM 0001-02) for TJ.

Author contributions

L.G.H. and L.D. designed the study, analyzed the data, and wrote the manuscript. A.C. designed the study. L.G.H. performed experiments with assistance of B.L., B.B. and N.C.; H.L., C.D. and

L.G. helped to analyze the results; T.J. analyzed the data and wrote the manuscript. M.B. and F.D. helped design the study; A.C. and L.D. supervised the study.

Competing financial interests:

L.G.H., C.D., T.J., L.G., L.D. and A.C. submitted a patent on the use of APLNR+ cell population to improve hematopoietic graft.

References

1. Doulatov, S., *et al.* Induction of multipotential hematopoietic progenitors from human pluripotent stem cells via respecification of lineage-restricted precursors. *Cell stem cell* **13**, 459-470 (2013).
2. Sandler, V.M., *et al.* Reprogramming human endothelial cells to haematopoietic cells requires vascular induction. *Nature* **511**, 312-318 (2014).
3. Sugimura, R., *et al.* Haematopoietic stem and progenitor cells from human pluripotent stem cells. *Nature* **545**, 432-438 (2017).
4. Lis, R., *et al.* Conversion of adult endothelium to immunocompetent haematopoietic stem cells. *Nature* **545**, 439-445 (2017).
5. Risueno, R.M., *et al.* Inability of human induced pluripotent stem cell-hematopoietic derivatives to downregulate microRNAs in vivo reveals a block in xenograft hematopoietic regeneration. *Stem cells* **30**, 131-139 (2012).
6. Swiers, G., Rode, C., Azzoni, E. & de Bruijn, M.F. A short history of hemogenic endothelium. *Blood cells, molecules & diseases* **51**, 206-212 (2013).
7. Antas, V.I., Al-Drees, M.A., Prudence, A.J., Sugiyama, D. & Fraser, S.T. Hemogenic endothelium: a vessel for blood production. *Int J Biochem Cell Biol* **45**, 692-695 (2013).
8. Sturgeon, C.M., Ditadi, A., Clarke, R.L. & Keller, G. Defining the path to hematopoietic stem cells. *Nature biotechnology* **31**, 416-418 (2013).
9. Slukvin, II. Deciphering the hierarchy of angiohematopoietic progenitors from human pluripotent stem cells. *Cell cycle* **12**, 720-727 (2013).
10. Lengerke, C., *et al.* Hematopoietic development from human induced pluripotent stem cells. *Ann N Y Acad Sci* **1176**, 219-227 (2009).
11. Ditadi, A., *et al.* Human definitive haemogenic endothelium and arterial vascular endothelium represent distinct lineages. *Nature cell biology* **17**, 580-591 (2015).
12. Yzaguirre, A.D., de Bruijn, M.F. & Speck, N.A. The Role of Runx1 in Embryonic Blood Cell Formation. *Advances in experimental medicine and biology* **962**, 47-64 (2017).
13. Van Handel, B., *et al.* Scl represses cardiomyogenesis in prospective hemogenic endothelium and endocardium. *Cell* **150**, 590-605 (2012).
14. Smadja, D.M., Cornet, A., Emmerich, J., Aiach, M. & Gaussem, P. Endothelial progenitor cells: characterization, in vitro expansion, and prospects for autologous cell therapy. *Cell biology and toxicology* **23**, 223-239 (2007).
15. Duttenhoefer, F., *et al.* 3D scaffolds co-seeded with human endothelial progenitor and mesenchymal stem cells: evidence of prevascularisation within 7 days. *European cells & materials* **26**, 49-64; discussion 64-45 (2013).
16. Tourino, C., *et al.* Efficient ex vivo expansion of NOD/SCID-repopulating cells with lympho-myeloid potential in hematopoietic grafts of children with solid tumors. *The hematology journal : the official journal of the European Haematology Association / EHA* **2**, 108-116 (2001).
17. Dick, J.E., Pflumio, F. & Lapidot, T. Mouse models for human hematopoiesis. *Semin Immunol* **3**, 367-378 (1991).
18. Kidoya, H., *et al.* Spatial and temporal role of the apelin/APJ system in the caliber size regulation of blood vessels during angiogenesis. *The EMBO journal* **27**, 522-534 (2008).
19. Yu, Q.C., *et al.* APELIN promotes hematopoiesis from human embryonic stem cells. *Blood* **119**, 6243-6254 (2012).
20. Peled, A., *et al.* Dependence of human stem cell engraftment and repopulation of NOD/SCID mice on CXCR4. *Science* **283**, 845-848 (1999).
21. Kollet, O., *et al.* Human CD34(+)CXCR4(-) sorted cells harbor intracellular CXCR4, which can be functionally expressed and provide NOD/SCID repopulation. *Blood* **100**, 2778-2786 (2002).
22. Nasrallah, R., *et al.* Endoglin potentiates nitric oxide synthesis to enhance definitive hematopoiesis. *Biology open* **4**, 819-829 (2015).

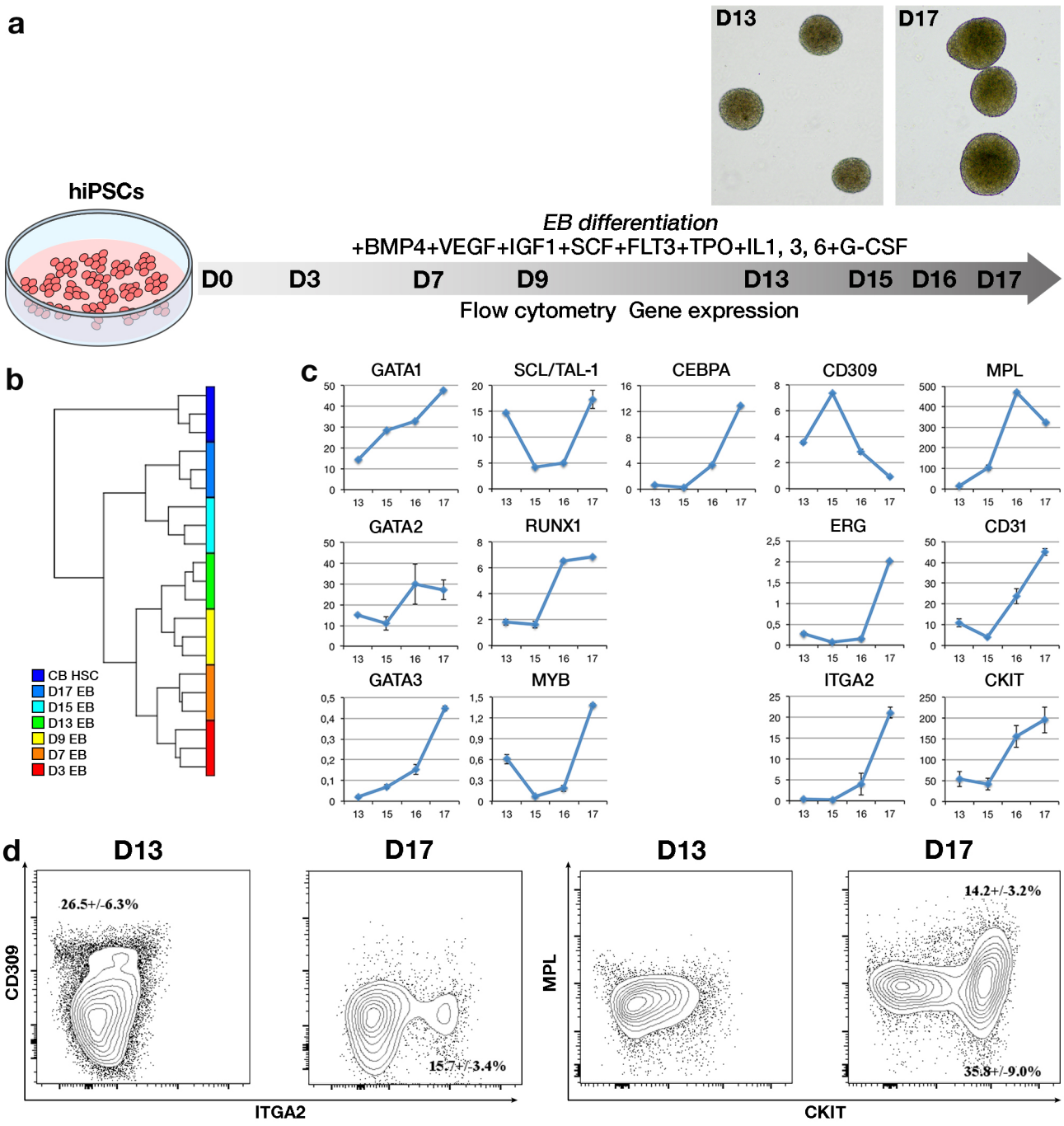

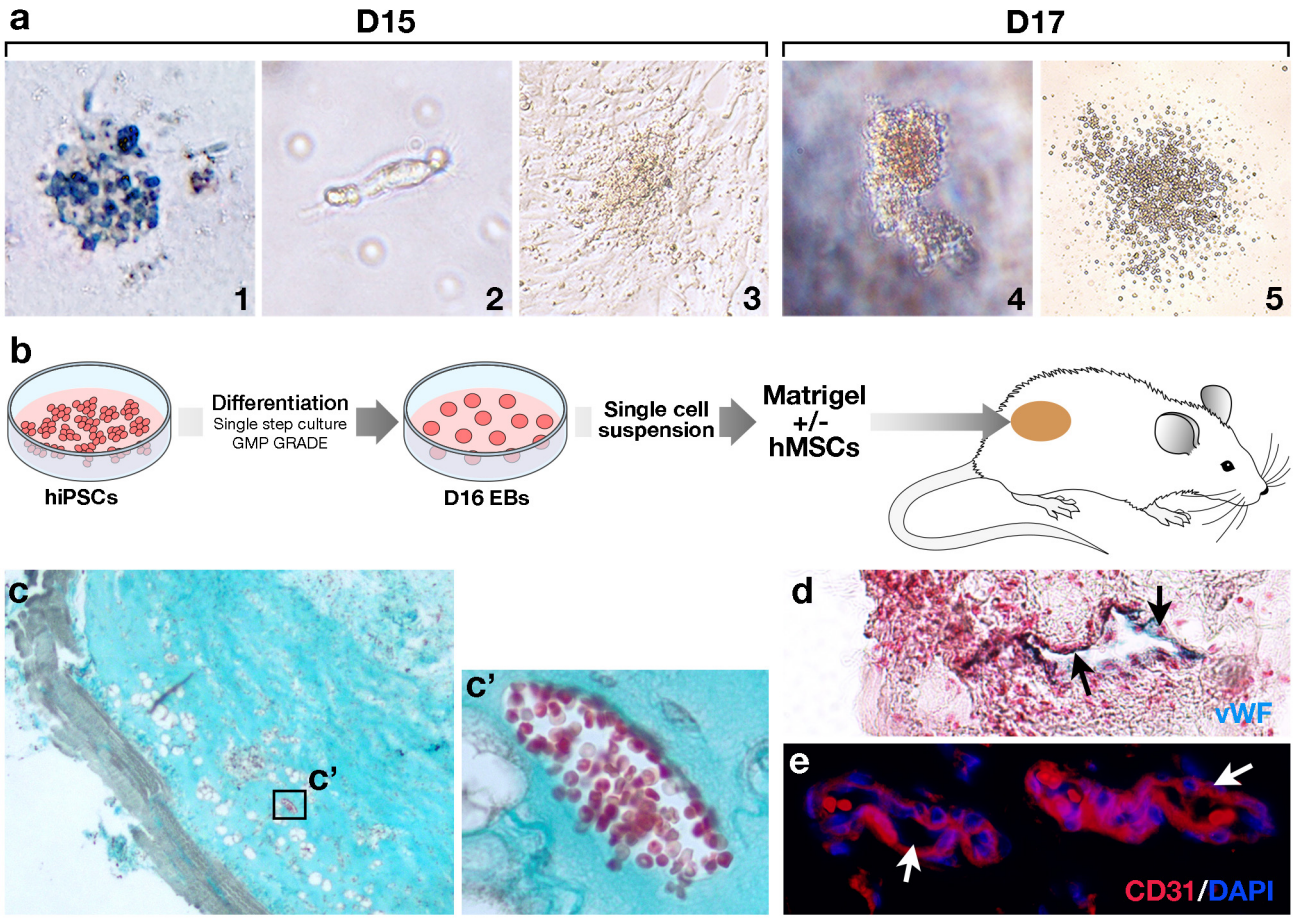

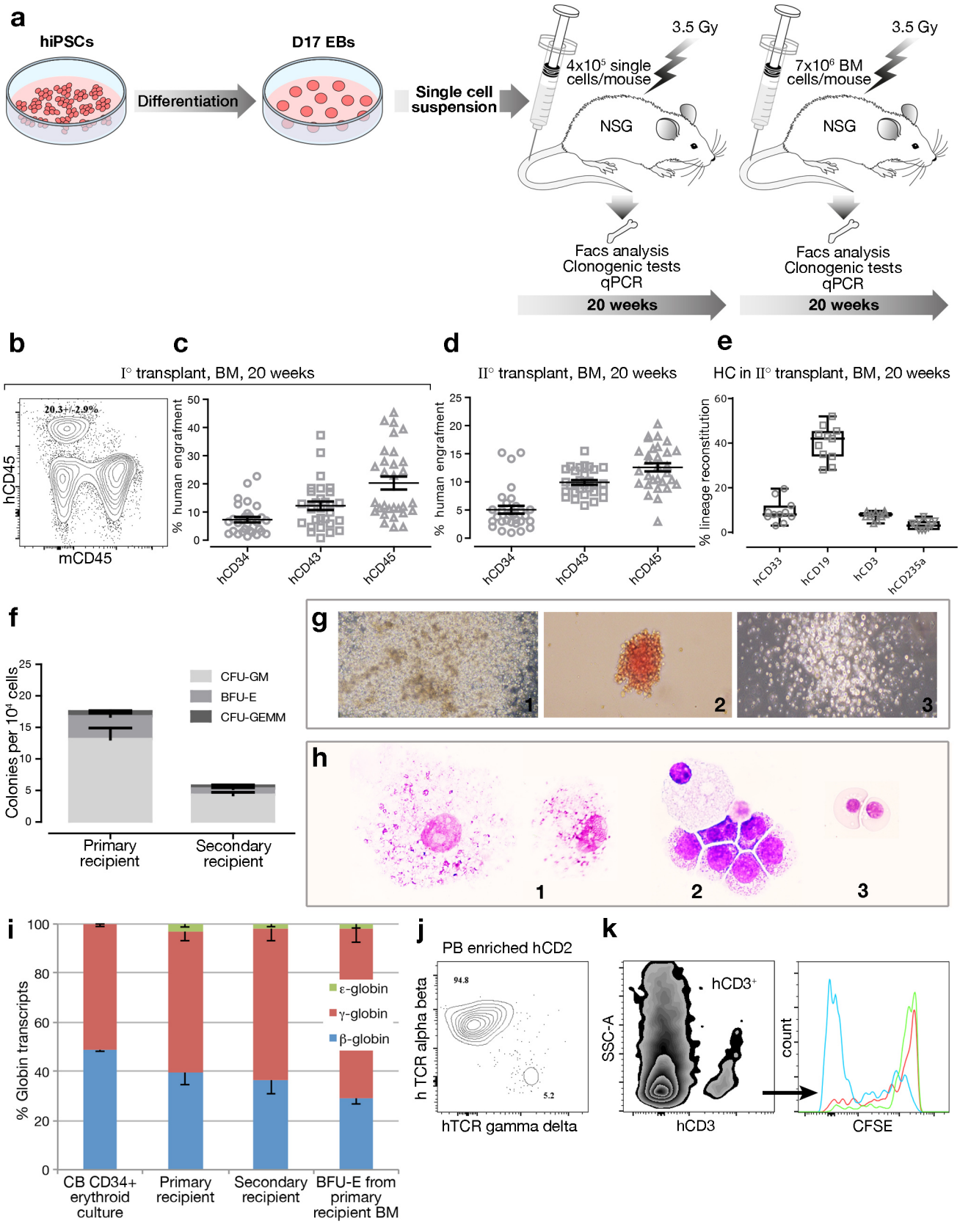

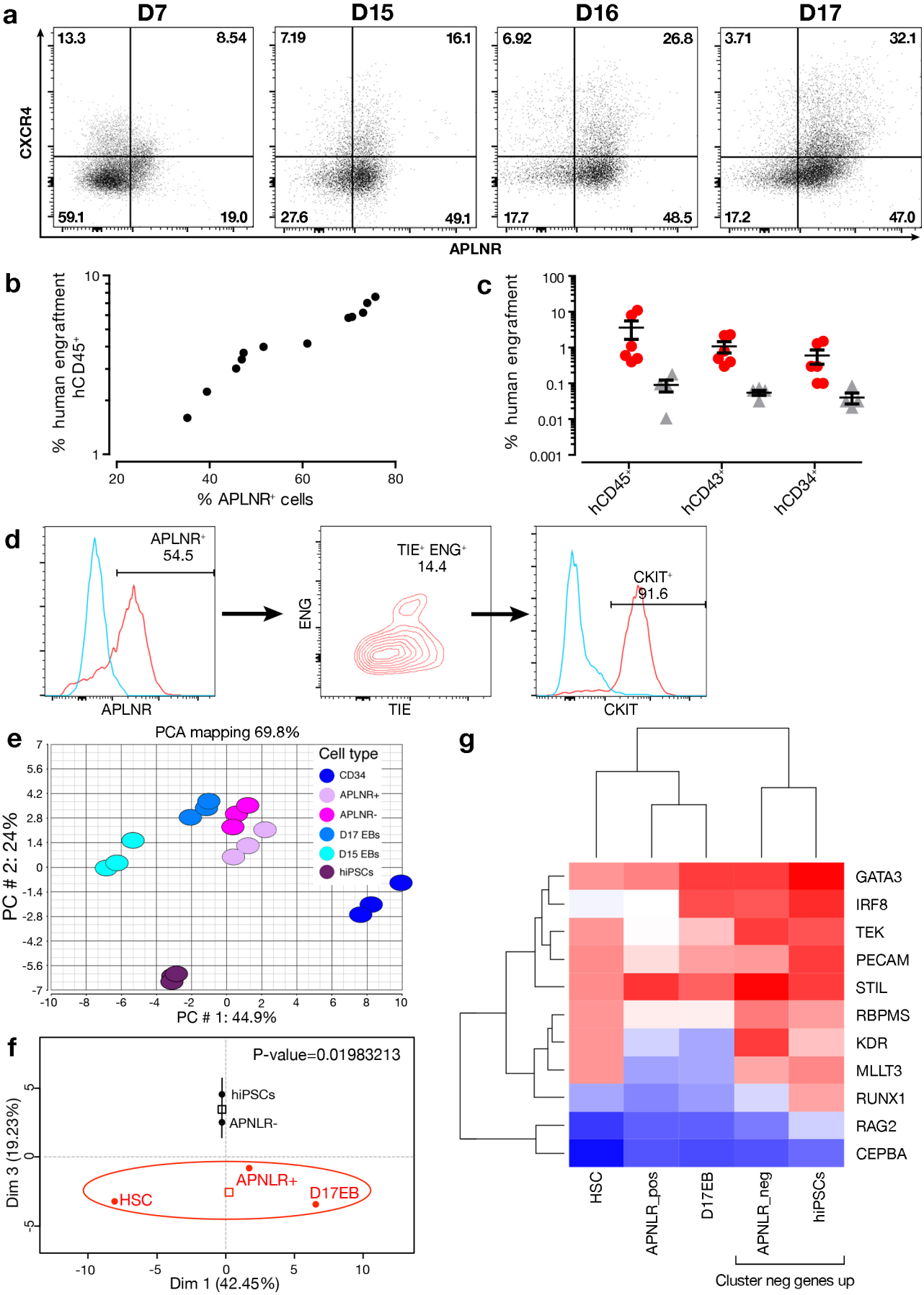

Supplementary information

Inventory of the supplementary figures and tables

Supplementary figure 1 is related to Figure 1

Shows the heat map of the gene list and the associated hierarchical clustering. It shows that $CD34^+$ cells form a first main branch and that the EBs are segregated in a second main branch. D3 to D13 EBs are separated from 1D5 to D17 EBs.

Supplementary figure 2 is related to Figure 2

Endothelial and hematopoietic potential carried by D16 EBs *in vivo*.

Supplementary figure 3 is related to Figure 3

It gives a complete overview of the analysis of the hematopoietic engraftment with representative examples of multilineage reconstitution.

Supplementary figure 4 is related to Figure 3

Bone marrow analysis of the hematopoietic engraftment, multilineage reconstitution of primary recipients.

Supplementary figure 5 is related to Figure 3

A complete overview of the hematopoietic multilineage engraftment of peripheral blood, thymus and spleen from D17 EB cell and CB $CD34^+$ HSPCs.

Supplementary figure 6 is related to Figure 3

Bone marrow analysis of the hematopoietic engraftment, multilineage reconstitution of secondary recipients.

Supplementary figure 7 is related to Figure 4

Characteristics of the $APLNR^+$ population in terms of hematopoietic engraftment.

Supplementary table 1 is related to Figure 1

Ex vivo endothelial and hematopoietic potential carried by hiPSC, HSC and D3 to D17 EBs.

Supplementary table 2 is related to Figure 2

Ex vivo endothelial and hematopoietic potential of EBs from D15 to D17.

Supplementary table 3 is related to Figure 4

Ex vivo endothelial and hematopoietic potential carried by hiPSC, CD34+ CB HSPC and APLNR+, APLNR- and D17 EBs.

Supplementary Figure 1

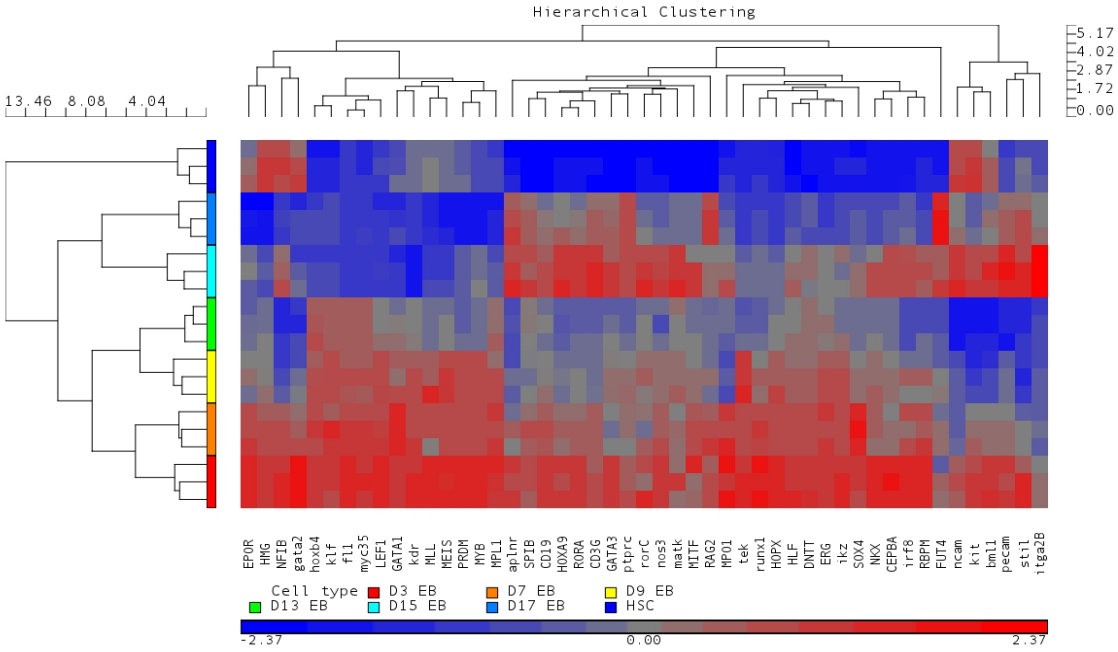

Supplementary Figure 2.

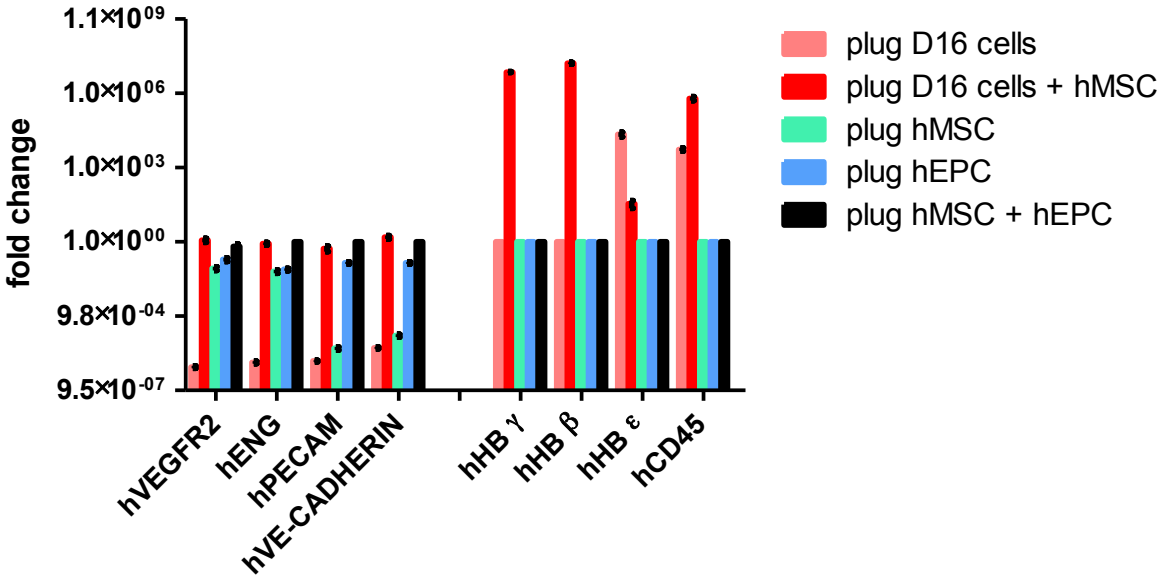

Supplementary Figure 3

a

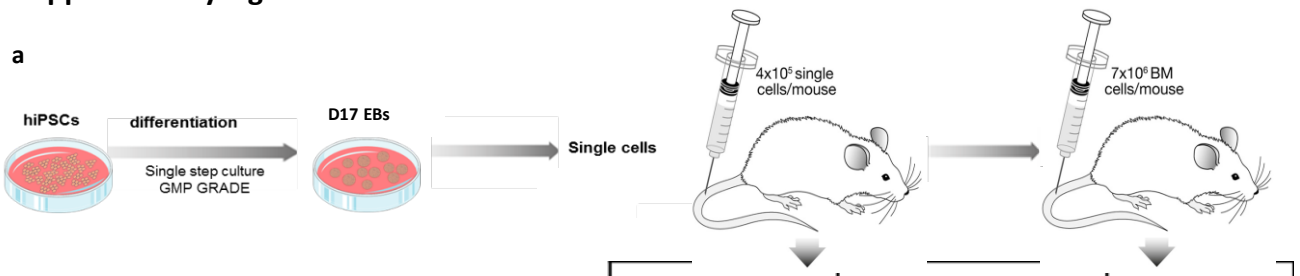

		culture	Facs analysis	qPCR human genes
Graft assessment	Total bone marrow		hCD45/mCD45 hCDd45/hCD43/hCD34	GAPDH
Multilineage assessment	hCD45 bone marrow sorting		hCD19 / hCD20 hCD14 / hCD15 hCD3 / hCD4 / hCD8	CD45 CD15 MPO ITGA2 GAPDH
	hCD45 blood sorting		hCD19 / hIgM hCD14 / hCD11B hCD3 / hCD4 / hCD8	
Stemness assessment	hCD45 bone marrow sorting	Colony assays		Beta globin Gamma globin Epsilon globin GAPDH
Definitive hematopoiesis assessment	Total bone marrow		hCD235a / hCD71	Beta globin Gamma globin Epsilon globin GAPDH
B and T cells functionality assessment	hCD45 blood sorting		TCR αβ ,TCR γδ	
	Thymus cells	CFSE labeling Stimulation with hCD3 and hCD28	hCD3/hCD4/hCD8	

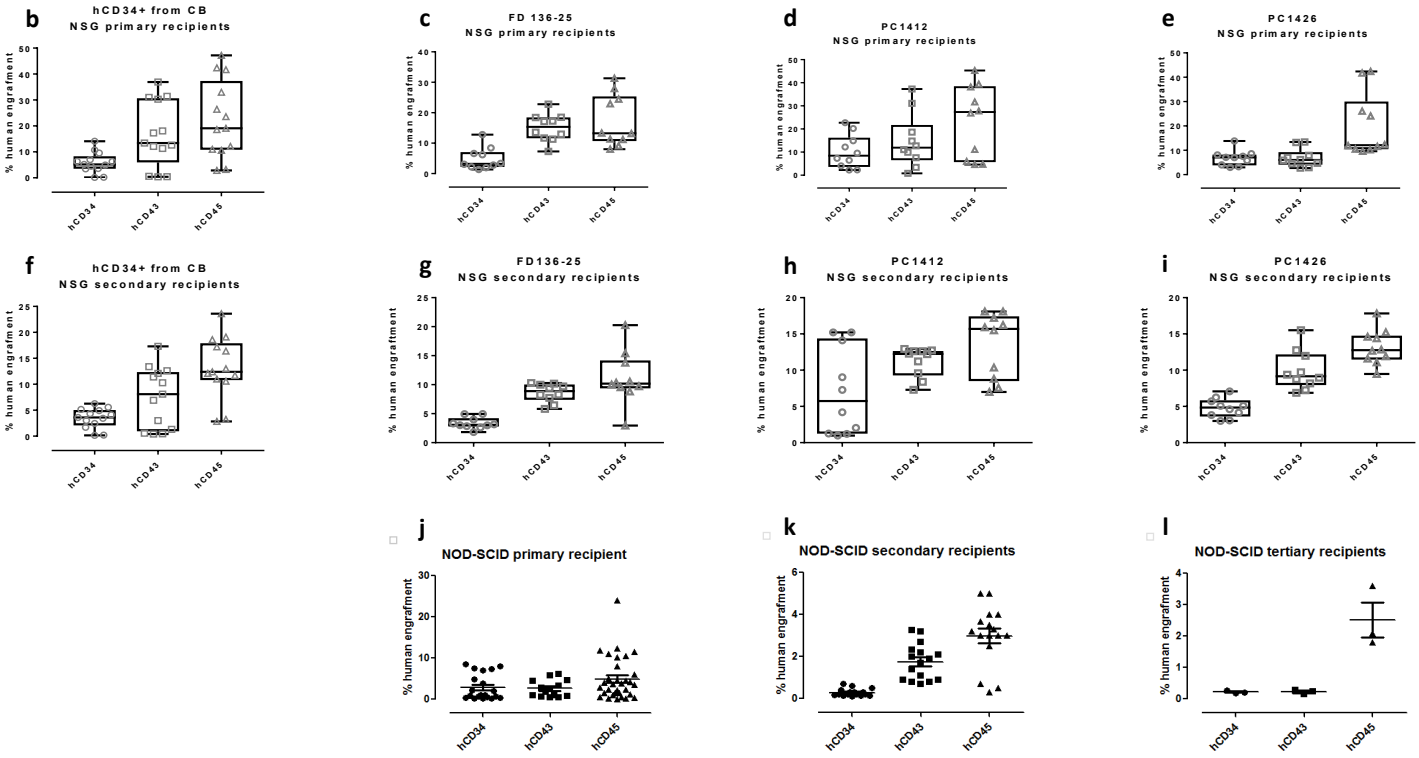

Supplementary Figure 4

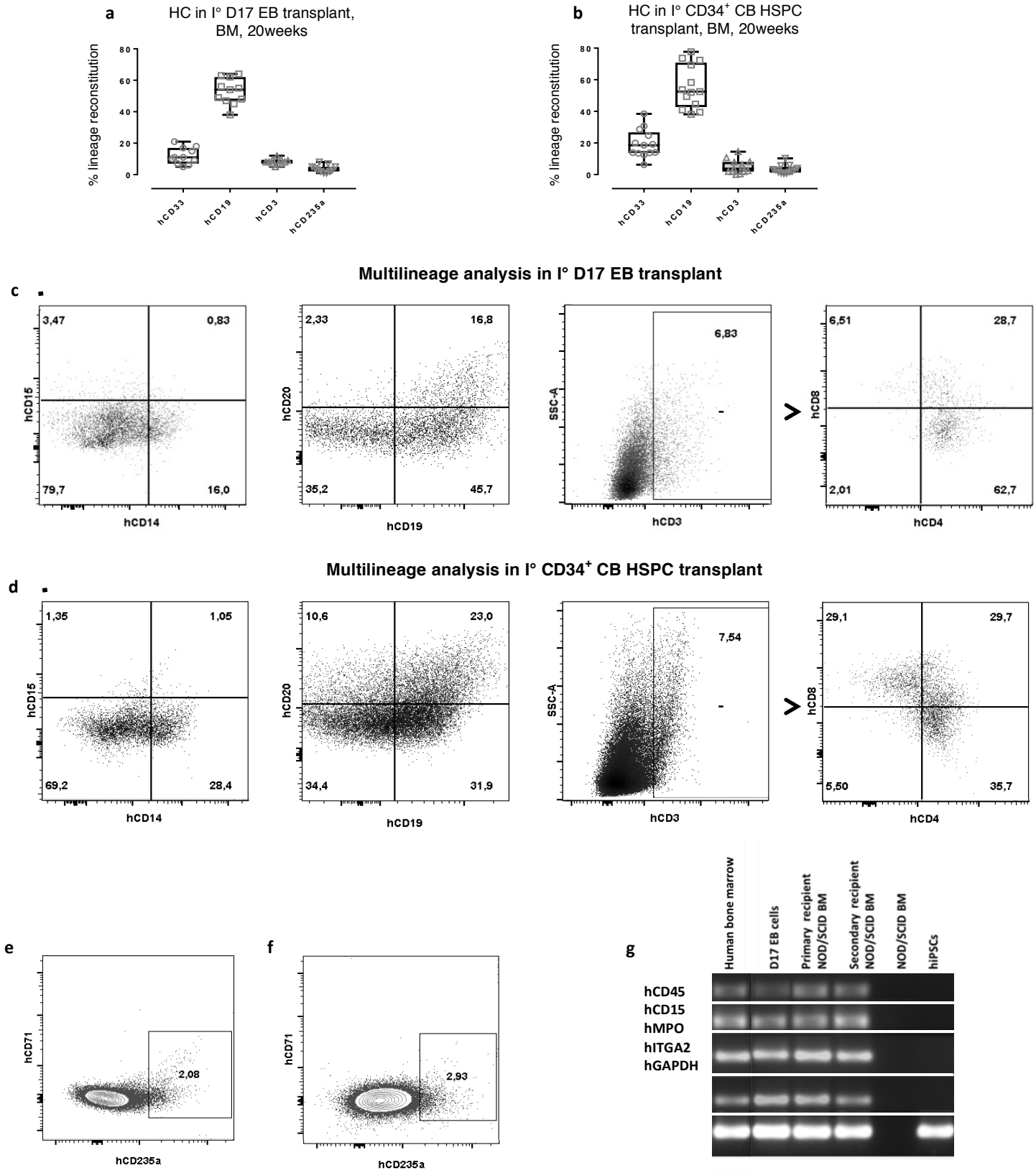

Supplementary Figure 5

a

Multilineage analysis peripheral blood

Ungrafted NSG

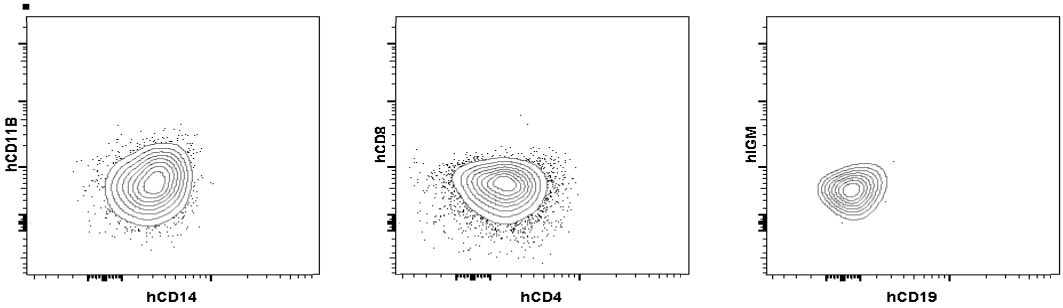

NSG I° D17 EB transplant

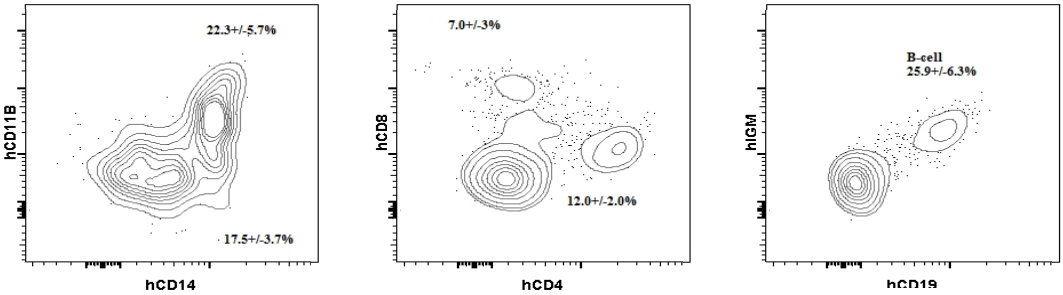

NSG I° CD34⁺ CB HSPC transplant

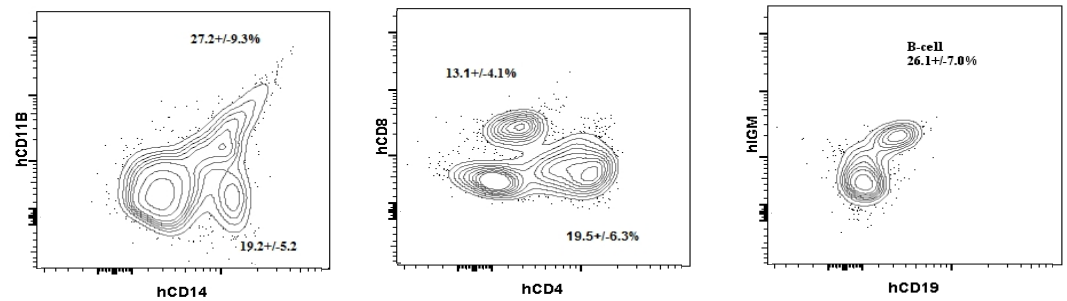

b

Multilineage analysis

Thymus **Spleen**

NSG I° D17 EBs transplant

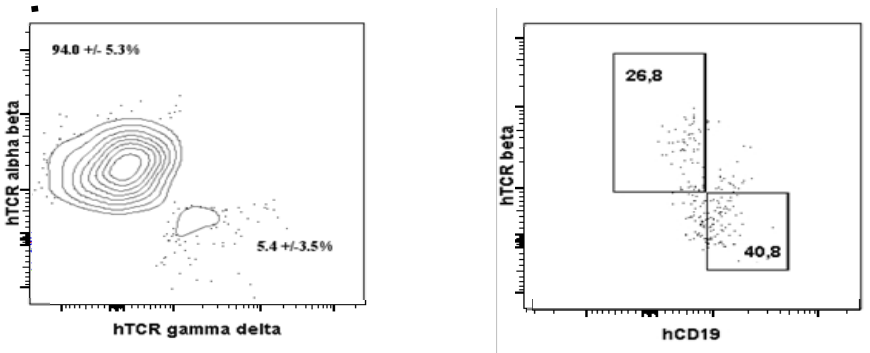

NSG I° CD34⁺ CB HSPCs transplant

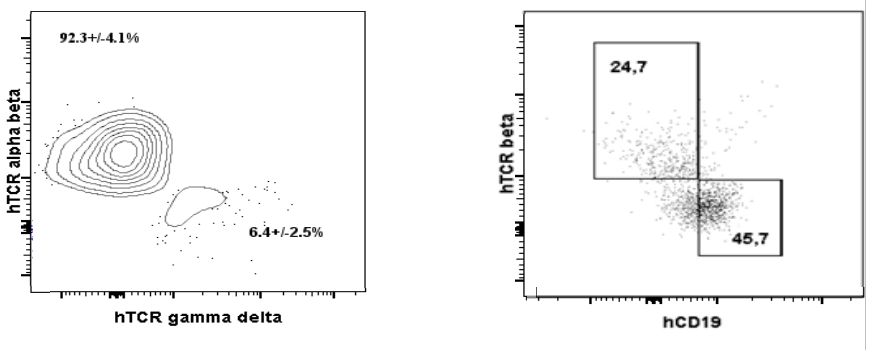

Supplementary Figure 6

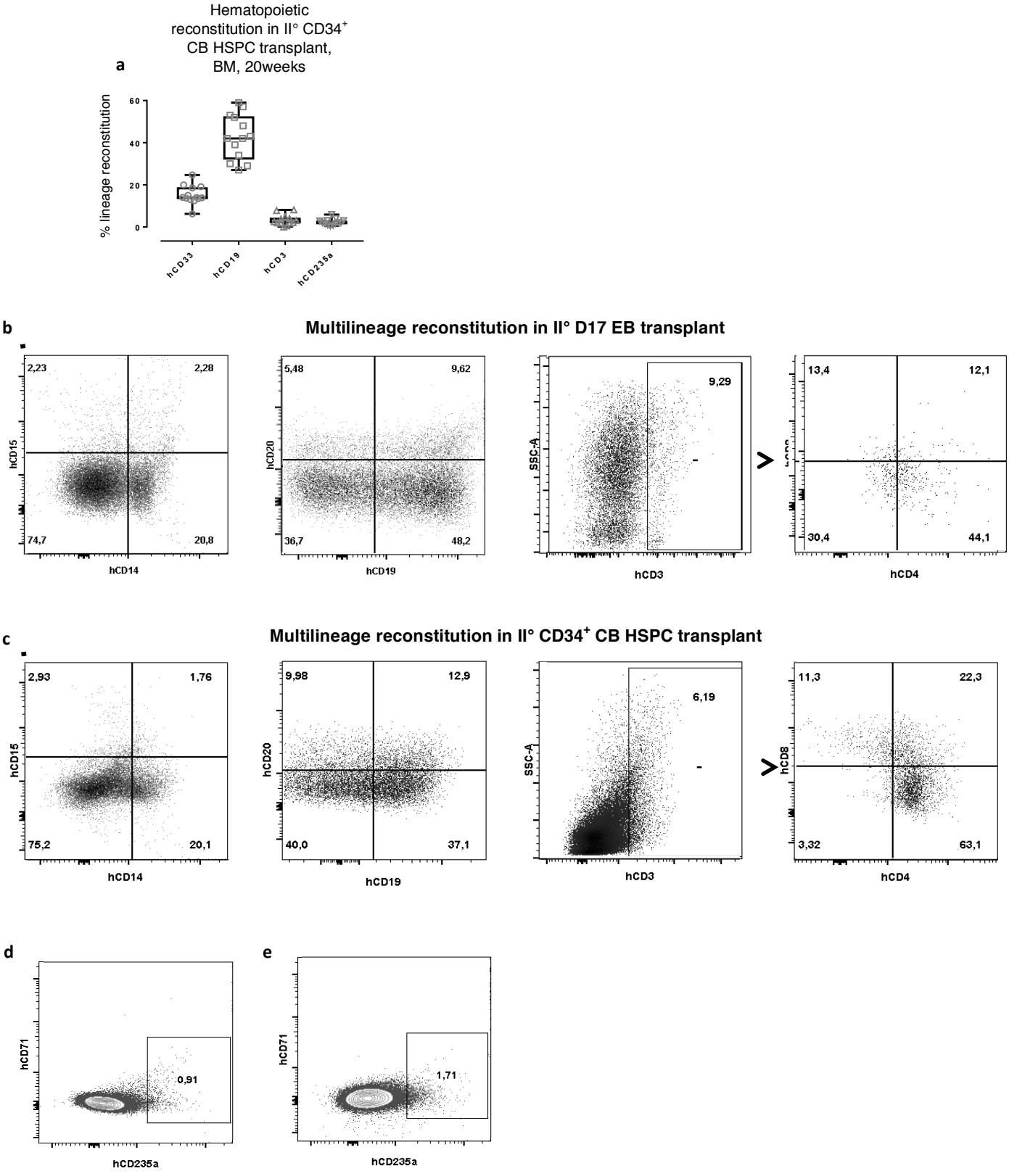

Supplementary Figure 7

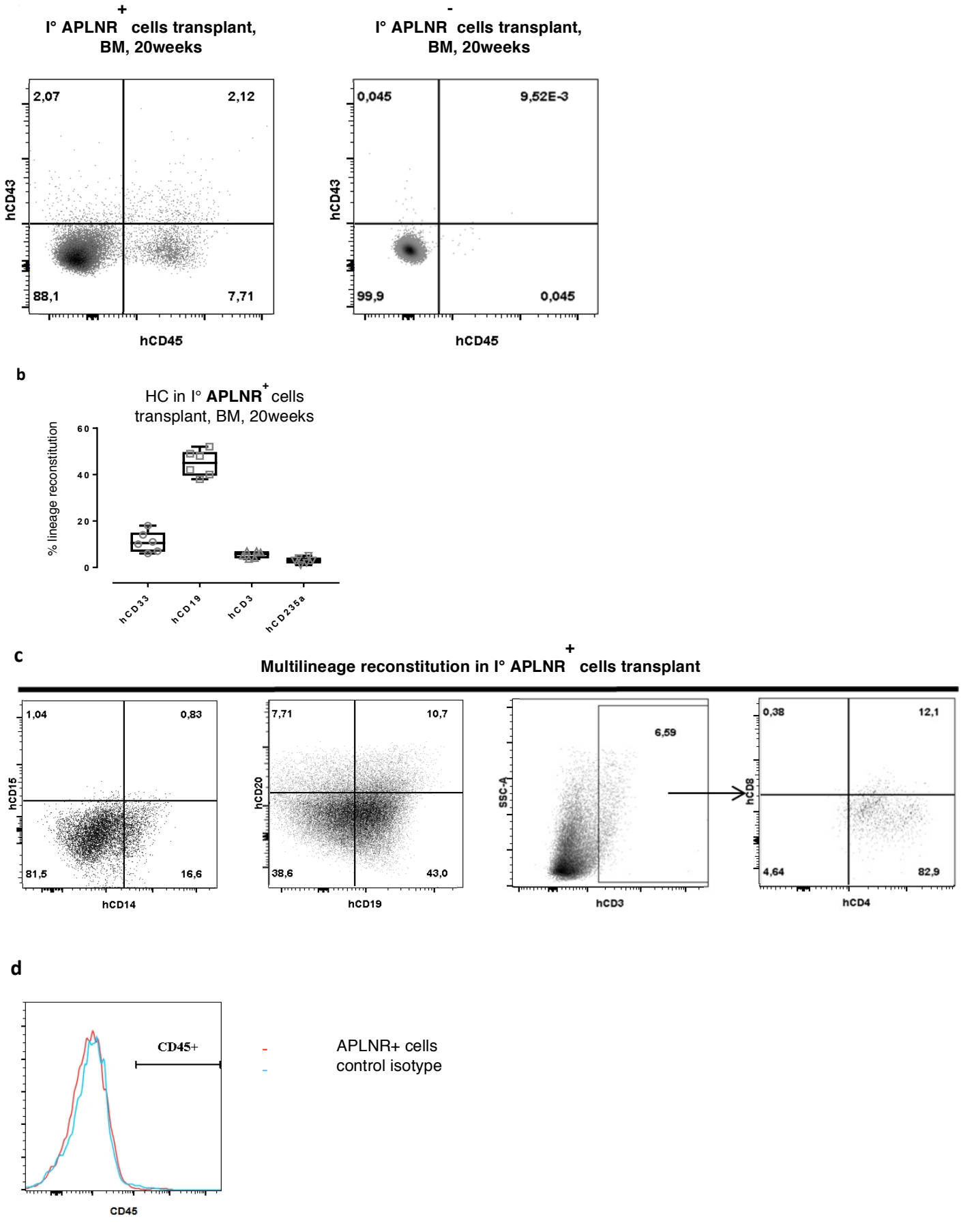

Supplementary Legends

Supplementary Figure. 1. Hierarchical clustering and principal component analysis of the set of 49 genes representative of endothelial and hematopoietic commitment.

Heat map of the gene expression and the associated hierarchical clustering. $CD34^+$ CB HSPCs are segregated from the EBs. D3 to D13 EBs are separated from D15 to D17 EBs.

Supplementary Figure 2. Endothelial and hematopoietic potential carried by D16 EBs *in vivo*.

Levels of expression of hVEGFR2, ENDOGLIN, PECAM-1, VE-CADHERIN, γ-globin, β-globin, ε-globin and CD45 in the matrigel plugs. For each gene, the fold change is the mean ± SEM of 3 independent experiments.

Supplementary Figure 3. *In vivo* engraftment of D17 human EBs in immunocompromised mice.

(a) Experimental design. The table summarizes the different tests and analyses performed on the hematopoietic populations.

(b-l) *In vivo* engraftment capacity in immunocompromised mice. (b) $CD34^+$ CB HSPCs in NSG primary recipient (n=13) at 20 weeks post-graft after inoculation of $2x10^5$ CD34+ cells. results are in % of $CD34^+$, $CD43^+$ and $CD45^+$ human cells. (c-e) D17 EBs from the three different hiPSCs lines (FD 136-25, PC1412 and PC1425) in NSG primary recipient (n=30) at 20 weeks post-graft after inoculation of $4x10^5$ D17 EBs. Results are in % of $CD34^+$, $CD43^+$ and

$CD45^+$ human cells. (f-i) Follow up of the secondary recipients (f) NSG secondary recipient at 20 weeks post-graft after inoculation of $7x10^6$ total BM cells from b. (g-i) NSG secondary recipient at 20 weeks post-graft after inoculation of $7x10^6$ total BM cells from respectively c, d, e. (j-l) Follow up of D17 EBs from the FD136-25 hiPSC line grafted in primary (e, $4x10^5$ cells, n=20), secondary (f, $7x10^6$ total BM cells, n=16) and tertiary (g, $7x10^6$ total BM cells, n=3,) NOD-SCID recipients. Results are in % of human $CD34^+$ $CD43^+$ $CD45^+$ cells in mouse BM at 20 (e), 20 (f) and 12 (g) weeks after transplant. Data are mean +/- SEM.

Supplementary Figure 4. Flow cytometry and qRT-PCR analysis of hematopoietic engraftment in primary BM recipients.

(a-b) Human hematopoietic cell lineages in primary recipients: (a) grafted with D17 EBs (n=30) and (b) grafted with $CD34^+$ CB HSPCs (n=13). Cells were gated on hCD45+ expression for hCD33, hCD19 and hCD3 whereas hCD235a was analysed on whole BM cells. Data are mean +/- SEM.

(c-d) Flow cytometry analysis for myeloid (hCD14/hCD15) and lymphoid (hCD19/hCD20, SSC-A/hCD3 and hCD4/hCD8) lineages from a representative NSG primary recipient grafted with D17 EB cells (c) or with $CD34^+$ CB HSPCs (d). Analyses were performed on $hCD45^+$ gated BM cells.

(e-f) Flow cytometry analysis of the erythroid lineage from a representative NSG primary recipient grafted with D17 EBs (e) or with $CD34^+$ CB HSPCs (f). Analyses were performed on whole BM cells.

(g) qRT-PCR analysis for hCD45, hCD15, hMPO, hITGA2 and hGAPDH expression in human BM cells (positive control), D17 EBs, NOD/SCID BM primary recipient grafted with D17 EBs, NOD/SCID BM secondary recipient, NOD/SCID BM ungrafted control, FD136-25 hiPSCs. PCR samples were run on several agarose gels. For presentation purpose, bands were assembled one above the other (white lines).

Supplementary Figure 5. Flow cytometry analysis of human hematopoietic lineages from representative primary recipients peripheral blood, thymus and spleen.

(a) Myeloid (hCD11B/hCD14) and lymphoid (hCD19/hIGM and hCD4/hCD8) lineages on peripheral blood of ungrafted recipient (1st line), of D17 EBs grafted recipient (2nd line) and of CD34^{+} CB HSPCs grafted recipient (3rd line). The analyses were performed on hCD45^{+} gated cells, aside the ungrafted recipient.

(b) Representative flow cytometry analysis of thymus and spleen cells. Thymus hCD3 gated cells exhibited a large amount of TCR alpha beta cells very close to that obtained using CD34^{+} CB HSPCs. hCD45^{+} gated spleen cells exhibited B or T lymphoid phenotype with ratios similar to those obtained with CD34^{+} CB HSPCs.

Supplementary Figure 6. Flow cytometry analysis of hematopoietic engraftment in secondary BM recipients.

(a) Human hematopoietic lineage distribution in secondary recipients grafted with 7.10^{6} whole bone marrow from CD34^{+} CB HSPCs-grafted primary recipient (n=13). Cells were

gated on hCD45+ expression for hCD33, hCD19 and hCD3 whereas hCD235a was analysed on whole BM cells. Data are mean +/- SEM.

(b-c) Flow cytometry analysis of the myeloid (hCD14/hCD15) and lymphoid (hCD19/hCD20, SSC-A/hCD3 and hCD4/hCD8) lineages. (b) From a representative NSG secondary recipient grafted with 7.10^6 whole BM from D17 EB primary recipient. Analyses were performed on $hCD45^+$ gated BM cells. (c) From a representative NSG secondary recipient grafted with 7.10^6 whole BM from $CD34^+$ CB HSPCs-grafted primary recipient.

(d-e) Representative flow cytometry analysis of the erythroid lineage. Analyses performed on whole BM cells. : (d) Representative NSG secondary recipient grafted with 7.10^6 whole BM of D17 EBs primary recipient and (e) Representative NSG secondary recipient grafted with 7.10^6 whole BM $CD34^+$ CB HSPCs-grafted primary recipient.

Supplementary Figure 7. Characterization of the $APLNR^+$ and $APLNR^-$ populations.

(a) Representative profile of hCD45 and hCD43 expression in mice BM grafted with either the D17 $APLNR^+$ (left) or $^-$ (right) cell fractions.

(b) Human hematopoietic lineage distribution in primary BM recipient grafted with $APLNR^+$ cells (n=6). Data are mean +/- SEM.

(c) Representative flow cytometry analysis of the myeloid (hCD14/hCD15) and lymphoid (hCD19/hCD20, SSC-A/hCD3 and hCD4/hCD8) lineages present in a primary BM recipient grafted with $APLNR^+$ cells.

(d) Representative flow cytometry analysis showing the absence of CD45 expression on APLNR$^+$ cells

Supplementary Tables

Supplementary Table 1. Ex vivo endothelial and hematopoietic potential carried by hiPSC, $CD34^+$ CB HSPC and D3 to D17 EBs.

Refer to the attached supptable1.xlsx file.

		Day 15 EBs (n=3)	Day 16 EBs (n=3)	Day 17 EBs (n=4)
Endothelial capacity	CFC-EC	+	-	-
	Pseudo-microtubules	+++	+	-
	EC's culture	++	+++	nd
EBs hematopoietic capacity versus $CD34^{+}CD45^{+}$ hematopoietic capacity	CFC	0	1/200	1/40
	CFC per LTC-IC	<1/600	1/15	1/4

Supplementary Table 2. Endothelial and hematopoietic potential carried by D15 to D17 EBs *ex vivo.*

EBs were probed for their capacities to give rise to either EC or HC colonies based on recognized functional tests. The highest endothelial potential was found at D15, markedly decreased at D16 and was absent at D17. In contrast, the hematopoietic potential was first detected at D16 and was high at D17.

Legend: EB: embryonic bodies; LTC-IC: Long Term Culture-Initiating Cells; CFC: Colony-Forming Cell.

Supplementary Table 3. Ex *vivo* endothelial and hematopoietic potential carried by hiPSC, $CD34^+$ CB HSPC and $APLNR^+$, $APLNR^-$ and D17 EBs.

Refer to the attached supptable3.xlsx file.

	hiPSC_1	hiPSC_2	hiPSC_3	D3 EBs_1	D3 EBs_2	D3 EBs_3	D7 EBs_1
D7 EBs_2	D7 EBs_3	D9 EBs_1	D9 EBs_2	D9 EBs_3	D13 EBs_1		D13
EBs_2	D13 EBs_3		D15 EBs_1		D15 EBs_2		D15
EBs_3	D17 EBs_1		D17 EBs_2		D17 EBs_3		CD34
HSPCs_1	CD34 HSPCs_2		CD34 HSPCs_3				
HOPX	7.3714	7.0732	6.6233	13.3164	13.2554	13.6364	10.5444
9.9853	9.7502	9.3740	8.8180	10.8621	6.7338	6.3784	7.1156
6.2102	6.0942	5.3418	2.9681	2.6392	2.2135	1.0406	0.7402
0.2861							
RBPM	4.0737	3.7816	3.4865	12.0818	12.0361	12.4018	10.0581
10.4622	11.1729	9.6973	7.8417	8.5548	7.9122	6.8338	6.8549
10.4894	10.0099	9.8023	6.7166	6.5380	5.9919	4.6664	4.6541
3.9029							
PRDM	6.2481	6.4327	5.7977	11.0850	11.0518	11.4050	9.0673
8.5028	9.2207	8.9212	8.3635	9.0746	4.7363	4.3735	4.4036
3.8602	4.1314	3.5279	−0.7339	−0.4540	−1.2654	4.4435	4.6541
3.8168							
NKX	8.9189	9.0755	8.4508	18.8239	18.6945	18.6562	14.5958
14.0516	13.6140	13.7424	13.2024	14.0354	12.1006	11.7649	11.8710
15.9205	16.2438	12.0193	9.4827	9.5973	8.8511	4.5224	4.6541
3.8908							
GATA3	10.2627	10.3681	9.8175	19.5774	19.9357	19.3531	13.6532
14.2512	14.8428	15.8103	15.1308	15.7498	14.8763	12.4039	13.5076
19.5109	20.1576	17.0843	16.3061	16.6025	15.8884	4.6664	4.7392
4.1292							
TEK	6.6877	6.9123	6.2624	13.1168	13.9377	14.3273	12.1146
11.6596	12.3660	13.7268	13.2512	13.9444	8.4572	7.1540	7.4739
8.6071	8.7656	7.9550	5.5029	5.7497	5.0712	4.6664	4.6541
4.1491							
NOS3	11.3284	11.7808	11.0486	19.1094	18.9764	18.6215	16.5221
15.9851	17.3272	15.5785	15.0454	15.2645	13.2662	12.9348	11.2083
18.3889	19.2071	18.2240	12.3298	12.8229	11.9933	4.6664	5.0028
4.3299							
MATK	5.4948	5.6179	5.0033	9.0663	9.6657	12.8194	9.7967
8.7035	9.7284	9.5438	9.3911	10.2241	8.3670	9.5993	8.7393
12.9506	13.3972	12.0185	7.9681	8.0673	7.4200	0.6980	0.8962
0.1638							
MITF	8.1788	8.4535	7.7597	19.5774	16.0575	16.0192	17.8103
16.8891	17.4936	15.8103	15.1308	15.9637	14.8763	14.4037	14.5437
18.4583	18.4342	14.8675	14.6030	14.4630	14.0920	8.4066	8.5481
7.8257							
HLF	10.0255	10.5624	9.7133	19.5774	19.9357	19.5477	17.8103
17.1308	17.8171	15.8103	15.1308	15.8171	14.8763	14.4037	14.3970
14.8994	16.1316	14.0049	11.1736	11.8465	11.1662	5.0447	5.5719
4.7440							
HMG	−1.3810	−1.6508	−1.9730	4.9250	4.9682	5.2449	3.5230
2.9381	3.6764	1.7828	1.1989	1.9362	1.3622	0.9870	
1.0296	−0.0661	−0.8822	−1.2771	−4.2257	−4.6088	−4.9812	4.6664
4.6541	4.3034						
MEIS	4.9645	5.4892	4.7154	11.0528	11.0199	10.6818	8.9966
8.4318	8.6233	9.4280	8.8722	9.4895	5.4137	5.0535	5.4066
1.4695	2.0969	1.1000	−0.9310	−0.3504	−1.2367	4.6664	5.1286
4.3607							
MLL	2.5769	3.4352	2.2761	9.8497	10.5028	10.1927	7.2192

```
7.1551   5.0987   6.9688   6.4897   10.6278  4.2281   3.5527   4.1243
0.1483   1.4081   0.4149   -0.7987  0.1009   -1.1079  4.6664   4.6541
4.2021
IRF8     9.1168   10.0666  9.0463   19.2218  19.9357  19.3586  13.9610
17.1308  16.6983  15.6409  11.1636  12.7477  9.3879   8.4117   8.8355
16.0534  17.0795  15.7855  10.7760  11.7956  10.6941  3.0656   4.2763
2.8577
RUNX1    4.5033   4.8527   4.0825   10.1772  10.1867  9.2439   7.7288
7.2491   7.4296   6.0467   4.7498   5.4420   3.9484   3.2351   3.3319
3.7874   4.0487   3.6351   1.8341   2.0904   1.3214   0.5525   0.9204
0.0752
KDR      0.3740   0.7412   0.0466   10.2469  11.5504  11.5122  9.3294
9.3478   10.1808  8.5188   7.9954   8.8284   5.7831   5.3568
5.4968   -2.5139  -2.4042  -2.5584  0.4948   0.8634   0.1555   4.6664
4.6541   4.2470
FLI1     5.2316   5.4024   4.7735   19.5774  19.9357  19.6188  17.8103
17.1308  17.7204  15.8103  15.1308  15.5266  14.8763  14.4037  14.5437
5.2316   5.4024   4.7735   5.2316   5.4024   4.7735   5.2316   5.4024
4.7735
MYC      1.2180   1.7649   0.9357   7.7928   7.6512   8.0825   5.8577
5.3499   6.5120   3.7102   2.8433   3.3566   2.9711   2.3159
2.8709   -7.9068  -8.1330  -8.7345  -7.9401  -7.4231  -8.2119  -10.0795
-9.5781  -10.3890
HOXB4    6.0216   6.1387   5.5368   8.6522   8.5261   8.2073   7.8336
6.8078   7.1817   5.8433   5.5142   6.8133   5.9547   5.0267
5.7937   -1.1602  -0.8976  -2.6499  -1.5792  -1.4416  -2.0085  -5.0263
-4.9096  -5.5225
NFIB     4.5185   4.4276   3.9068   8.2167   8.8587   8.5744   7.0850
6.8654   7.6433   3.9541   2.8493   4.2543   2.8547   1.8207   2.1265
6.4076   7.5474   6.0778   3.3816   3.1509   2.6873   8.0706   7.3624
7.1720
RAG2     3.2504   3.3148   2.7597   1.7425   2.2910   3.0163   2.6533
2.0198   3.5713   0.5403   -0.6392  -0.4012  -0.5334  -1.1539  -0.8860
0.4973   0.4935   -0.0518  3.3718   3.2147
2.7047   -7.0681  -7.4822  -7.5066
SPIB     -2.2027  -2.1636  -2.7222  14.1956  13.4104  13.7933  13.8401
12.1497  13.3049  9.9993   10.1805  10.8849  10.7524  11.1396  11.1450
13.5194  16.2929  13.8033  12.6414  12.6288
12.0653  -0.8492  -0.2420  -0.9642
SOX4     10.4954  10.1914  9.1848   15.7257  15.6348  16.0457  17.8103
16.7660  17.4537  13.4747  12.9338  13.6281  12.2670  11.9319  11.9343
13.7376  13.2264  12.3050  11.4967  11.2336  10.1767  8.2218   7.7004
6.8193
MYB      5.7862   5.7702   5.1635   15.2467  15.1617  15.1235  12.9687
12.4185  13.2515  12.9298  12.3869  13.2198  9.0614   8.7145   8.8545
9.4659   9.6166   9.4207   3.2386   3.2335   2.5982   7.4350   7.3877
6.7525
HOXA9    12.6539  13.6803  12.1869  19.5774  19.9357  19.0150  17.8103
17.1308  16.8642  15.8103  15.1308  15.4163  14.8763  14.4037  14.0700
20.1234  21.5431  19.3669  16.4051  17.4507  15.9109  9.3995   10.2691
8.8499
ERG      5.8874   6.2409   5.4849   14.4151  15.5593  15.5210  13.0553
14.5256  15.3585  12.6419  11.9463  12.7792  9.9676   9.9155   10.0555
9.3980   9.8957   9.4470   4.6106   5.1559   4.2727   0.0409
```

```
0.3615  -0.3499
RORA    12.6885 13.2743 11.6565 19.5774 19.9357 19.6007 17.8103
17.1308 17.8171 15.8103 15.1308 15.8171 14.8763 14.4037 14.3970
20.2953 20.4542 19.5193 16.4397 17.0447 15.4431 8.8263  9.4026
7.7562
LEF1    3.3233  3.0408  2.4735  10.2337 10.2111 10.5537 8.3351
7.7679  8.4885  8.1420  7.5815  8.2954  4.7258  4.3630
4.3932  -0.0990 -0.1473 -1.1553 -1.1492 -1.4735 -2.0176
0.4274  -0.1945 -0.5986
CEPBA   3.6455  3.4011  3.0264  8.2969  8.2983  8.8644  2.7402
2.1524  2.8936  2.8535  2.2736  2.8620  1.1825  0.8066  0.9023
5.1752  5.1549  5.1464
0.0303  -0.2396 -0.5983 -4.7972 -5.0360 -5.4256
EPOR    6.5140  6.0491  5.6933  11.4750 11.1677 11.5333 10.0831
9.5224  10.3553 8.4187  8.0356  7.5322  7.4411  7.0232  7.3219
7.9699  6.9438  7.6577  4.4829  3.8647  3.5703  8.5875  9.1469
7.5455
GATA1   8.7722  10.4808 8.0736  16.3199 16.2091 16.0201 17.8103
17.1308 17.4407 12.4171 13.2872 14.4484 12.2203 10.4666 11.9413
7.0414  7.0511  5.2609  6.2853  7.6878  5.1171  8.9147  10.8537
8.2660
IKZ     6.6242  6.7153  6.1183  12.3638 12.8589 13.6536 11.1133
10.8750 11.0953 10.8082 9.8302  10.6631 8.8854  7.1990  7.3390
7.6197  8.3593  9.0394  5.9941  5.4902  5.3246  2.9345  1.9589
1.8899
KLF     11.4937 12.1131 11.1870 16.7194 16.1611 16.8892 17.8103
14.4879 16.9322 15.8103 15.1308 15.4761 14.8763 14.4037 14.5437
9.8417  10.3439 9.0712  9.8299  10.1432 9.3468  6.6165  6.6930
6.0229
MPL1    12.9788 13.8778 12.1867 18.3643 17.9191 18.0651 16.3234
17.1308 17.8566 15.8103 14.1328 15.7409 14.8763 14.4037 13.9442
11.0722 11.7014 10.2042 6.9502  7.7831  6.1766  9.8195  9.9893
8.5215
NCAM    12.8672 13.5782 12.6086 6.5597  6.7878  7.1229  4.0498
3.4408  4.1262  3.7648  2.5405  3.5555  -0.0298 -0.1206 -0.4468
8.8082  9.7399  8.6319  5.1943  5.6921  4.9720  7.8237  8.5147
7.5085
PECAM   17.0334 17.0891 16.3635 13.0888 12.9874 12.3399 10.7956
10.3021 11.0177 9.6331  8.7304  9.5323  5.6790  5.7804  6.1118
14.9788 14.7874 14.3060 11.5790 11.5794 10.8030 7.8595  7.9270
7.1646
PTPRC   9.1821  9.2906  8.7038  7.4861  8.3684  6.8817  6.7439
6.1671  5.9121  6.6060  5.9549  6.7878  4.6872  4.0338  4.1738
8.2761  8.4459  7.8949  8.4380  8.4207
8.1129  -1.1682 -1.0555 -1.6517
RORC    15.5461 15.8810 14.6577 16.7992 19.1554 15.6776 14.3420
15.0846 16.2194 15.8103 15.1308 15.0568 14.8763 14.4037 14.5437
18.2071 18.6152 17.2936 14.1428 14.6540 13.1596 9.2457  9.6241
8.3088
FUT4    4.5133  5.3964  4.3866  -0.0675 2.2475  2.5189  1.9334
1.0635  2.4434  1.7881  0.4176  1.8154  -0.0623 -0.5931 -0.5400
3.0826  4.1432  2.8111  6.4065  6.5130
5.7509  -3.4111 -2.5714 -3.6297
APLNR   17.0324 17.5544 16.1144 16.0328 15.8920 15.5785 14.7484
```

13.2436 13.8934 13.2144 11.7176 12.7121 12.1808 11.8383 12.2783
16.5968 17.1793 15.4520 15.5791 16.1511 14.6163 9.8259 10.3607
8.8922
BMI1 17.0457 16.8117 16.0815 8.2926 8.8724 8.6128 6.7697
6.2378 7.0344 4.6903 3.8838 5.1331 3.2223 2.5242 2.7022
8.9816 8.6204 8.1051 6.6656 6.5258 5.7374 7.5189 7.2786
6.5403
ITGA2-B 11.0373 11.6504 10.8464 6.6302 7.1970 7.4826 5.9472
5.3028 5.1924 5.1226 4.0247 5.0200 4.1307 3.6185 3.9329
13.1184 13.4129 13.0793 6.6071 7.1950 6.4328 4.1531 4.7657
3.9557
MPO1 12.5047 13.5649 12.1909 15.3298 15.2683 13.8288 12.7473
13.2782 14.2574 7.9865 7.1271 7.6882 8.6489 8.9153 8.9926
10.7283 12.2185 10.1319 8.0890 9.2884 7.6140 4.9503 5.9813
4.6180
STIL 16.3427 16.1914 15.1624 8.7871 10.3516 10.3236 7.8353
7.0348 7.6268 4.7592 5.7768 5.6189 5.5032 5.0863 5.0633
10.6395 10.7712 9.1835 9.3565 9.2100 8.2109 7.5237 7.3526
6.3377
KIT 13.6601 13.9053 13.2368 6.0285 6.3778 6.3449 4.9774
4.5186 5.4457 2.7680 2.0804 3.0100 1.6865 1.3571 1.4477
6.1602 6.6672 5.9113 3.8607 4.2344 3.5268 6.6609 6.9222
6.2251
GATA2 10.4935 10.8050 9.6199 9.8459 10.1980 10.1597 7.9024
7.1197 7.9526 6.5856 5.4597 6.6480 5.4874 5.0709 4.3838
6.1647 6.3061 5.0153 5.2388 5.4945 4.3228 8.2535 8.4898
7.2164
CD19 15.1001 15.2333 13.5740 19.5774 19.9357 19.7970 17.8103
17.1308 17.2897 13.6412 13.2544 15.0616 10.5852 11.9274 13.2127
17.7611 17.9675 16.2099 13.6967 14.0062
12.0759 -2.3351 -2.2501 -4.0246
CD3G 16.0572 15.2338 14.0264 14.6337 15.0801 15.0419 13.6808
13.6161 14.4490 11.3041 10.5380 11.3710 10.8488 9.3107 9.4507
18.7183 17.9679 16.6178 14.6039 13.8305 12.5283 3.0172 2.1854
0.9678
DNTT 15.1001 13.8089 15.1624 19.5774 19.9357 19.7770 17.8103
17.1308 17.4201 15.8103 15.1308 15.8063 14.8763 14.4037 14.5437
14.6277 13.0667 14.6228 10.7456 9.1485 10.6705 4.1302 2.1332
3.6867

	hiPSCs	APNLR+	APNLR−	D17 EBs	CD34 HSPCs
CMYC	6.23	5.04	4.58	4.21	6.66
HOXB4	8.52	6.52	5.58	4.57	6.66
LIN28	−1.89	1.54	2.04	−2.89	−7.25
NANOG	−2.38	1.71	2.77	0.68	−9.33
POU5F	−6.44	2.96	1.48	3.42	−8.11
SOX2	−3.02	0.37	0.76	2.71	−8.13
FUT4	−2.85	2.94	4.19	0.24	−4.59
APNLR	9.80	10.43	12.16	15.19	7.00
BMI1	9.80	7.46	6.32	6.23	7.00
ITGA2B	3.54	6.48	4.70	6.66	1.54
MPO1	5.23	4.81	5.92	7.41	7.00
STIL	9.80	10.15	11.72	8.54	7.00
KIT	7.91	4.40	3.01	4.02	7.00
GATA2	9.80	7.12	6.10	7.38	5.51
CD19	9.80	10.43	12.16	17.00	−0.90
CD3G	9.80	10.43	12.16	14.13	7.00
NCAM	5.42	4.55	2.60	4.50	7.00
PECAM	9.80	5.11	6.54	6.36	7.00
PTPRC	1.43	8.82	8.08	5.42	−2.89
RORC	9.80	10.43	12.16	17.02	7.00
ERG	9.31	6.26	9.52	10.62	3.18
GATA3	11.81	7.40	9.77	9.78	6.66
HOXA9	9.31	7.84	9.77	10.66	4.61
IRF8	10.45	4.50	8.88	9.27	4.33
KDR	5.58	3.71	9.77	2.90	6.66
MITF	6.74	7.41	8.55	5.44	6.66
MLLT3	7.16	2.57	6.06	2.93	6.66
RBPMS	6.41	4.79	7.63	4.78	6.66
RUNX1	6.17	0.36	3.81	2.01	2.98
TEK	9.05	4.52	9.77	5.59	6.66
HMG	0.10	−0.16	−0.29	8.69	6.66
HOPX	7.72	4.97	4.49	12.11	2.71
LEF1	6.21	4.57	5.98	9.50	4.61
MEIS	6.72	4.10	3.71	8.09	6.66
MYB	6.21	7.03	6.71	12.30	4.61
NKX	8.61	7.73	6.71	13.66	6.66
PRDM	7.28	2.69	2.04	7.66	6.66
NOS3	9.73	7.73	5.46	9.55	6.66
SOX4	5.90	7.73	5.46	6.98	3.61
CEPBA	−1.83	−3.41	−3.45	−4.20	−8.86
HLF	9.10	7.73	5.46	10.47	6.66
RORA	5.90	7.73	5.46	10.47	4.61
EPOR	6.64	6.64	3.22	6.86	3.05
GATA1	12.99	7.96	6.79	10.16	7.06
IKZ	8.58	6.35	5.98	8.66	6.19
KLF1	12.17	13.84	5.12	13.17	4.57
MATK	10.83	8.93	5.93	9.28	2.80
MPL1	16.29	11.74	6.79	13.12	6.08
NFIB	4.84	3.32	2.21	3.43	4.61
RAG2	3.64	−2.64	−0.40	−2.60	−5.56
SPIB	−1.82	11.27	6.79	11.31	−3.65
HLF	9.10	7.73	5.46	10.47	6.66